International Journal of Solids and Structures 45 (2008) 4147–4172

Contents lists available at ScienceDirect

International Journal of Solids and Structures

journal homepage: www.elsevier.com/locate/ijsolstr

Intra-granular plastic slip heterogeneities: Discrete vs. Mean Field approaches

S. Berbenni *, M. Berveiller, T. Richeton

Laboratoire de Physique et Mécanique des Matériaux, LPMM, UMR CNRS 7554, ENSAM, Technopole, 4, rue Augustin Fresnel, 57078 Metz Cedex 03, France

ARTICLE INFO

Article history:
Received 2 October 2007
Received in revised form 18 January 2008
Available online 13 March 2008

Keywords:
Plasticity
Dislocations
Crystals
Microstructural
Micro-mechanics

ABSTRACT

In this paper, we derive the mechanical fields (internal stresses, elastic energy) arising from the presence of an inelastic distortion field representing a typical intra-granular "microstructure" as the one observed during the plastification of metallic polycrystals. This "microstructure" is due to the formation of discrete intra-granular plastic slip heterogeneities characterized by at least two internal lengths: the first one is the individual grain size which represents a stochastic parameter inherent to the processing route (prior working, annealing), and, the second one is the spatial distance between active slip lines or slip bands associated with inhomogeneous plastic slip in the interior of grains. These internal lengths can be observed and measured using conventional experimental techniques (EBSD, TEM, AFM). The micro-mechanical modeling of the mechanical fields associated with plastic slip events inside grains is performed with two different assumptions. The first one is based on the well-known Eshelby's problem of plastic inclusion where only the grain diameter is considered as internal length scale. This classical method considers homogeneous plastic distortion in the grain and leads to a uniform and grain size independent total strain field in the grain. The second method accounts for a non-uniform plastic distortion in the grain characterized by its discrete nature and the two aforementioned internal lengths. Both methods consider grains as spherical inclusions with a given diameter embedded in a homogeneous medium. For the second method, plastic slip is constrained by grain boundaries seen as impenetrable obstacles to dislocations. Thus, plastic strain is embodied by distributions of discrete circular glide loops. After writing the field equations and the free energy of the medium, a micro-mechanical formulation based on the Fourier transform method is developed. It is then found that in contrast with the mean-field approach, the internal stress fields as well as the elastic energy corresponding to different dislocation configurations depend on internal lengths associated to the deformed medium. Different possible configurations associated with intra-granular plastic flow due to circular glide dislocation loops are analyzed. Finally, the results are discussed with respect to the grain size dependence of the flow strength and the Bauschinger effect for plastically deforming polycrystals and perspectives to develop new micro–macro transition schemes accounting for internal length scales are sketched out.

1. Introduction

The determination of the inelastic behavior of heterogeneous materials with complex microstructures constitutes a challenge in the design of advanced materials (e.g. alloy design in the metallurgical industry) and the modeling of their effective

* Corresponding author. Tel.: +33 3 8737 5430; fax: +33 3 8737 4284.
E-mail address: Stephane.Berbenni@metz.ensam.fr (S. Berbenni).

0020-7683/$ - see front matter © 2008 Elsevier Ltd. All rights reserved.
doi:10.1016/j.ijsolstr.2008.02.028

behavior during their processing. Volume fractions, crystallographic and morphologic orientations but also sizes and shapes of the grains are constitutive elements of the microstructure of heterogeneous materials (metals, ceramic, intermetallics, etc.) which have to be tailored. In polycrystals, grain size corresponds to the initial microstructure obtained after complex material forming and recrystallization processes. Thus, such internal length is inherent to the initial microstructure and does not evolve significantly except for very large strains (grain shape evolution).

In Berbenni et al. (2007a,b), we investigated the role of grain size distribution on the yield stress of heterogeneous materials using an elastic–viscoplastic self-consistent model based on the translated fields technique (Sabar et al., 2002; Berbenni et al., 2004). In this modeling, the viscoplastic strain rate followed a power law including a phenomenological grain size-dependent reference stress of Hall–Petch type. As a result, we well-captured supplementary stored energy and internal stresses due to grain size heterogeneities. Grain size dispersion effects were found to be of first order on the macroscopic yield stress for fine grained materials (i.e. for materials with average grain size on the order of μm). Nevertheless, we assumed in this description a classic mean-field approach for grains so neglecting the strong inhomogeneity of plastic slip and especially its discrete nature. Here, we are seeking to determine how the grain size effect is related to the initial microstructure and the induced intra-granular plastic heterogeneities.

On the experimental point of view, the spatial heterogeneity of plastic flow was first highlighted through the observation of the surface of metals which indicated that slip consists of discrete events localized along slip bands (Neuhäuser, 1983). Deformation patterns emerging at the surface can be observed during tensile or compression tests on single crystals and polycrystals with large grains as well as fine grains for a variety of metals using experimental techniques such as EBSD or AFM (Brinck et al., 1997; Villechaise et al., 2002; Zaiser et al., 2004; Cai et al., 2005; Fréchard et al., 2006). The slip steps observed on the surface of these materials manifest the cooperative motion of dislocations leading to a highly localized deformation. In situ observations of these slip events can be performed through acoustic emission measurements which gives information about the dynamics of plastic flow (Miguel et al., 2001). The collective role of discrete dislocations on the internal mechanical fields is then found to be predominant. Measurements on ice single crystals and on various kinds of metallic single crystals (Richeton et al., 2006) indicate that plastic deformation proceeds through intermittent discrete slip events ("dislocation avalanches") with scale-free size distribution. However, in the case of ice polycrystals, a breakdown of this scale-free behavior was observed due to a complex grain size effect (Richeton et al., 2005).

On the modeling point of view, classical crystal plasticity models do not account for both length scale effects and boundary conditions for discrete slip. First contributions (Aifantis, 1987, 1992, 1995) linked the presence of characteristic internal length scales to gradient terms in the local constitutive equations of the grains. In the statistical theory of Zaiser and Seeger (2002) and Zaiser and Aifantis (2006), fluctuations in the local flow stress lead to strain fluctuations which in turn give rise to long range stress redistribution. Dislocation–dislocation correlations are statistically calculated and lead to a supplementary local back stress which can be related to the second-order strain gradient.

In this paper, we demonstrate that other contributions on internal stress and elastic energy – than the ones provided by the methods based on the Eshelby's solutions – are captured when the discrete and collective nature of slip is taken into account. More specifically, we describe the intra-granular plastic heterogeneity by circular glide loops as the carriers of discrete quantas of plastic slip, respectively, represented by spatial Dirac distribution functions. Thus, intra-granular plastic strain or plastic distortion arising from dislocations are no more considered homogeneous and uniform as in classic mean-field approaches in continuum mechanics such as the self-consistent model. Hence, this work is also a break with the classic Eshelby's framework of the uniform plastic inclusion, considering the case of strongly heterogeneous and discrete plastic events within grains. In Section 2, we present the general theory starting from the description of discrete plastic fields and the field equations of the problem. The mean-field approach based on the classic Eshelby inclusion is briefly recalled. In Section 3, the Fourier transform method for general *eigenstrains* is detailed. In Section 4, the applications to discrete plastic fields are presented. In a first attempt, we will consider single-slip situations for different grain sizes where glide loops, embedded within a spherical grain, have a given Burgers vector and are separated by a constant distance making the dislocation distribution periodic. Glide loops are considered since they develop in the glide plane from Frank-Read sources. From the data given by Neuhäuser (1983), observed slip line patterns (e.g. in pure f.c.c. crystals) are more or less homogeneous after the onset of plasticity (stage I for single crystals) and gradually slip bands occur (under a more localized plastic deformation especially from the stage II of single crystals). Therefore, we will consider periodic distributions of single dislocation loops for the sake of simplicity. In Section 5, we will focus numerical results on the influence of grain size and spatial period of loops on internal stress fields and internal free energy. These results are then discussed to establish a new way to account for internal lengths in micro–macro models. This way appears to be intermediate between full discrete dislocation dynamics simulations (Kubin et al., 1992; Verdier et al., 1998; Schwarz, 1999; Khraishi and Zbib, 2002) which become rapidly time consuming for polycrystals, and, generalized continua approaches which introduce internal length scales through new degrees of freedom like in strain gradient plasticity (Shu and Fleck, 1999) or in Cosserat media (Forest et al., 2000). Throughout this paper, we will study the influence of internal lengths as parameters characterizing static configurations of dislocations. These parameters will be bounded by physical values. It is not the scope of the present study to account for the system evolution. The present method allows us to consider other configurations such as periodic distributions of parallel clusters of loops which can represent slip bands. It is noteworthy that the same kind of calculations can be applied to fatigue since in the specific case of cyclic deformation, the slip patterns are found to present a quasi-periodicity (Zaiser and Seeger, 2002). The concept of clusters of loops presented here may be extended to describe persistent slip bands in fatigue. The findings of the present paper give new insights regarding the grain size dependence of the flow strength and the Bauschinger

effect in polycrystals. The presented method could serve as the basis of a statistical theory in order to treat the case of real polycrystalline materials for which both intra- and inter-granular effects are in competition.

2. General background

2.1. Inelastic distortion fields and dislocations

Considering the framework of small perturbations of deformed materials, the total distortion $\boldsymbol{\beta}$ (i.e. the displacement gradient which is compatible) splits into two contributions at any position vector $\mathbf{x}$:

$$\boldsymbol{\beta}(\mathbf{x}) = \boldsymbol{\beta}^{e}(\mathbf{x}) + \boldsymbol{\beta}^{in}(\mathbf{x}), \tag{1}$$

where $\boldsymbol{\beta}^{e}$ is the (incompatible) elastic distortion of the lattice and $\boldsymbol{\beta}^{in}$ is an (incompatible) inelastic distortion. This last one may have various physical origins which lead to different internal structures more or less controlled by crystallography. For example, the Bain deformation present in martensitic transformations is due to an inelastic lattice distortion which affects some volume elements. In the case of plasticity of metals at room temperature, the inelastic (i.e. plastic) distortion results from discrete glides of crystallographic planes (in directions given by Burgers vectors) due to dislocation motions which conserve crystal lattice. These elementary deformation mechanisms have a significant role on the macroscopic mechanical behavior of metals. Here, we consider first the description of the plastic distortion associated to a single dislocation loop, then, we treat an ensemble of dislocations.

2.1.1. Single dislocation loop

Let us consider a dislocation loop L formed by a cut in the material over a surface S bounded by L (Fig. 1). For the sign convention, we have chosen following Peach and Koehler (1950) and Kröner (1958) the surface normal $\mathbf{n}$ and the line vector $\mathbf{t}$ to respect the right-hand rule. Therefore, Fig. 1 shows the positive sense of the outward normal $\mathbf{n}$ and the positive sense of the Burgers circuit, i.e. the closed curve encircling the dislocation line. Now, the displacements are constructed by displacing the upper side of surface S (denoted S^+ with unit normal $\mathbf{n}^+ = \mathbf{n}$) by Burgers vector $\mathbf{b}$ with respect to the lower side of surface S (denoted S^- with unit normal $\mathbf{n}^- = -\mathbf{n}$) and then gluing them together.

Thus, the expression of the plastic distortion field $\boldsymbol{\beta}^{*}(\mathbf{x})$ induced by the dislocation loop L described on Fig. 1 is singular on the surface S and its expression reads according to Kosevich (1979):

$$\beta^{*}_{ji}(\mathbf{x}) = b_i n_j \delta(\mathbf{S}), \tag{2}$$

where $\delta(\mathbf{S})$ is a shorthand notation for the Dirac delta function in the direction $\mathbf{n}$, i.e. infinite when $\mathbf{x}$ is on S and zero elsewhere:

$$\delta(\mathbf{S}) \equiv \int_S \delta(\mathbf{x} - \mathbf{x}')\, \mathrm{d}S(\mathbf{x}'). \tag{3}$$

This first representation of a dislocation loop as described above is due to Volterra (1907). Experimentally, dislocation loops can be observed and their densities can be measured using high-resolution microscopes (TEM) or atomic force microscopes (AFM). Therefore, dislocations represent the state of the crystal and their density is a state variable of the medium (Kröner, 1958; Kroupa, 1962). In order to build up a relevant theory of plasticity accounting for heterogeneous slip due to dislocation motion, we have to express the free energy of the medium with dislocations as a function of quantities characterizing the dislocation distributions. Considering dislocation density as state variable holds for one dislocation as well as for dislocation ensembles, namely a given distribution of dislocations. By integrating around the loop L enclosing the surface S (Fig. 1), the change in plastic distortion field embodied by the Burgers vector b_j can be written with the help of the Stokes theorem:

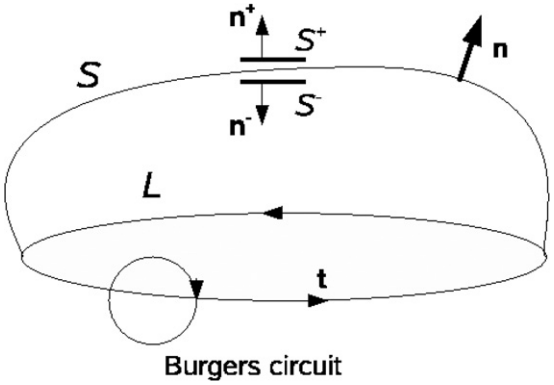

Fig. 1. Dislocation loop L formed after cutting the material over a surface S.

$$b_j = -\oint_L \beta^*_{ji}\,\mathrm{d}x_i = -\int_S \in_{ilm}\beta^*_{mj,l}\,\mathrm{d}S_i = \int_S \alpha_{ij}\,\mathrm{d}S_i, \tag{4}$$

where $\boldsymbol{\alpha}$ is the dislocation density tensor or Nye tensor (Nye, 1953):

$$\alpha_{ij} = -\in_{ilm}\beta^*_{mj,l}. \tag{5}$$

In Eqs. (4) and (5), symbol $\in_{ilm}$ denotes the Levi-Civita tensor (also called permutation tensor). A direct consequence of Eq. (5) is that **div** $\boldsymbol{\alpha} = 0$ in V. In the above description (Fig. 1), the Burgers vector **b** can be written as an integral over the surface S:

$$b_j = \int_S t_i b_j \delta(\mathbf{l})\,\mathrm{d}S_i, \tag{6}$$

where $\delta(\mathbf{l})$ is a shorthand notation for the Dirac delta function in the plane perpendicular to the dislocation line vector **t**. Thus, comparing Eq. (4) with Eq. (6), the Nye tensor for a single dislocation is also defined as:

$$\alpha_{ij} = t_i b_j \delta(\mathbf{l}). \tag{7}$$

The discrete plastic mechanism described for a single dislocation can be easily generalized to an ensemble of dislocations as discussed now.

2.1.2. Dislocation ensembles

When the material deforms plastically during external loadings, a large number of dislocations move collectively in single or multiple slips forming sub-structures at the meso-scale like glide lines or glide bands depending on the crystallographic structure of the material. According to Neuhäuser (1983), the formation of slip lines is due to the correlated motion of several dislocations which generally takes a few milliseconds and slip bands are developing after the correlated formation of several slip lines.

Regarding dislocation ensembles, the question is whether some averaged characteristics of dislocation distributions or plastic distortion fields can be used. In the case of classical crystal plasticity, the inelastic fields are described by plastic distortions which read:

$$\overline{\boldsymbol{\beta}^*}(\mathbf{x}) = \sum_s \mathbf{m}^{(s)} \otimes \mathbf{n}^{(s)} \gamma^{(s)}, \tag{8}$$

where $\otimes$ is the dyadic product, $\gamma^{(s)}$ is an average plastic slip on slip system (s), $\mathbf{n}^{(s)}$ and $\mathbf{m}^{(s)}$ are, respectively, the unit vector normal to the slip plane and the unit vector in the glide direction. According to Kröner (1958, 1960), it is possible to associate a *quasidislocation* density $\overline{\boldsymbol{\alpha}} = -$**curl** $\overline{\boldsymbol{\beta}^*}$ to an average plastic distortion $\overline{\boldsymbol{\beta}^*}$. Actually, this density of quasidislocations does not correspond to true dislocations. Indeed, the details about plastic fields are lost when the derivation (due to the **curl** operator) is directly performed on the average field.

During the plastification of polycrystals, experimental observations show that dislocations are largely stored in grain boundaries. They are mainly constituted of geometrically necessary dislocations (the so-called GNDs as introduced by Ashby (1970)) which are present to accommodate the strong strain gradients associated with lattice incompatibility. Grain boundaries constitute crystalline interfaces (due to the misorientations between grains) and consequently are strong obstacles to dislocation motion. Furthermore, mutual interactions between dislocations lead to intra-granular structures (forest dislocations, slip bands, etc.) in the interior of grains mainly under the form of statistically stored dislocations (or SSDs). Therefore, the plastic distortion $\boldsymbol{\beta}^*(\mathbf{x})$ or the true dislocation density $\boldsymbol{\alpha}(\mathbf{x})$ are very complex functions.

In the representation based on quasidislocations (i.e. the *mean field approach*), $\overline{\boldsymbol{\alpha}}(\mathbf{x})$ is zero in the grain interior volume, and, is non-zero and uniform only on the surfaces delimited by grains (i.e. on grain boundaries). Considering now an isolated grain as a simple plastic inclusion of uniform plastic distortion $\overline{\boldsymbol{\beta}^*}^{\mathrm{I}}$ embedded in an infinite plastic matrix of uniform plastic distortion $\overline{\boldsymbol{\beta}^*}^{\mathrm{M}}$, then the plastic distortion jump is $\Delta\overline{\boldsymbol{\beta}^*} = \overline{\boldsymbol{\beta}^*}^{\mathrm{I}} - \overline{\boldsymbol{\beta}^*}^{\mathrm{M}}$ which gives rise to the surface quasidislocation tensor $\overline{\boldsymbol{\alpha}}^S$ as follows:

$$\overline{\alpha_{ij}}^S = \in_{ilm}\Delta\overline{\beta^*_{mj}}\, n_l, \tag{9}$$

where **n** is unit normal vector on the surface directed towards the infinite medium from the grain. This concept of surface dislocation density was introduced by Bullough and Bilby (1956) and the general theory of continuous distribution of dislocations was developed by Kröner (1958, 1960, 1966, 1981) to derive the internal stresses.

In the representation based on discrete glides on a slip system characterized by **n** and **m** (i.e. the *discrete approach*), the plastic distortion writes using Eq. (2):

$$\beta^*_{ji} = \sum_n b_i^{(n)} n_j^{(n)} \delta(\mathbf{S}^{(n)}), \tag{10}$$

where (n) denotes a given dislocation loop of surface $S^{(n)}$. Thus, the application of Eq. (5) to the last equation yields $\alpha_{ij} = \sum_n t_i^{(n)} b_j^{(n)} \delta(\mathbf{l}^{(n)})$ with the same notations as previously. In this approach, the knowledge of the microstructure (Burgers vectors, spatial distribution of discrete dislocations) and the associated internal lengths are needed to determine the static solutions for internal stresses and free energy. In order to compare both approaches, the average of the plastic dis-

tortion corresponding to the discrete distribution will be the same as the uniform plastic distortion used in the mean-field approach. This kind of study has been performed by Mura (1964) and Saada and co-workers (Rey and Saada, 1976; Saada, 1979, 2006; Saada and Bouchaud, 1993) on planar periodic dislocation arrays. They showed that long range internal stresses due to the discrete distribution of straight dislocations reduce to internal stresses obtained by using the average continuous distribution of interfacial dislocations. Close to the plane of the dislocation array, a difference occurs where the solution given by the discrete distribution decreases exponentially with the distance to the array to tend to the solution of the average continuous distribution. Furthermore, this exponential decrease depends on the period of the array. In Section 4, some distributions of discrete glide dislocation loops spreading in a spherical grain will be considered assuming single slip situations. The role of grain size on internal stresses and elastic energy will be examined. Different configurations will be treated from a relative "homogeneous" slip when dislocations spread homogeneously and periodically along the grain to more "localized" slip when loops gather in clusters across the grain. These original results will be interpreted in comparison with those obtained by the classical hypothesis of uniform plastic distortion in the spherical grain, i.e. the classical Eshelby's framework. The discrete approach may also be extended to multiple slip configurations.

2.2. Field equations and thermodynamics

Let us consider an individual spherical inclusion (the considered grain) with volume V_g embedded in an infinite matrix with volume $V \gg V_g$ (i.e. unbounded material). We assumed no volume force and isothermal conditions in the medium. Furthermore, quasi-static loading is assumed. Symbol ":" will denote the contracted product between two tensors and symbol "·" will denote simple product.

On the boundary ∂V of V, a prescribed displacement $\mathbf{u}^d$ (Dirichlet conditions) is considered:

$$\mathbf{u}^d = \mathbf{E}\cdot\mathbf{x} \quad \text{on} \quad \partial V, \tag{11}$$

where $\mathbf{E}$ is a uniform imposed strain on ∂V.

The other field equations are constituted of:

- the stress equilibrium condition for the symmetric Cauchy stress tensor $\boldsymbol{\sigma}$:

$$\mathbf{div}\ \boldsymbol{\sigma} = 0 \quad \text{in} \quad V, \tag{12}$$

- the compatibility relation for total distortion $\boldsymbol{\beta}$ and total strain $\boldsymbol{\epsilon}$ where $\mathbf{u}$ is the displacement field:

$$\boldsymbol{\beta} = \nabla\mathbf{u} \quad \text{and} \quad \boldsymbol{\epsilon} = \frac{1}{2}\left(\nabla\mathbf{u} + \nabla^t\mathbf{u}\right), \tag{13}$$

so that the associated total distortion $\boldsymbol{\beta}$ splits into two terms:

$$\boldsymbol{\beta} = \boldsymbol{\epsilon} + \boldsymbol{\omega}, \tag{14}$$

where $\boldsymbol{\omega}$ is the rotation.

- the total strain (respectively, the total distortion) in the small perturbation hypothesis writes as the sum of an elastic strain $\boldsymbol{\epsilon}^e$ (respectively, elastic distortion $\boldsymbol{\beta}^e$) and a plastic strain $\boldsymbol{\epsilon}^*$ (respectively, plastic distortion $\boldsymbol{\beta}^*$) which will be described for various representations, namely discrete vs. mean-field approaches:

$$\begin{aligned} \boldsymbol{\beta} &= \boldsymbol{\beta}^e + \boldsymbol{\beta}^*, \\ \boldsymbol{\epsilon} &= \boldsymbol{\epsilon}^e + \boldsymbol{\epsilon}^*, \end{aligned} \tag{15}$$

- the constitutive equation for elasticity (assumed homogeneous and linear):

$$\boldsymbol{\sigma} = \mathbf{C} : \boldsymbol{\epsilon}^e = \mathbf{C} : (\boldsymbol{\epsilon} - \boldsymbol{\epsilon}^*), \tag{16}$$

where $\mathbf{C}$ denotes the homogeneous elastic moduli. In this problem, the unknown fields are the displacement $\mathbf{u}$, from which the total distortion $\boldsymbol{\beta}$, and, the stress $\boldsymbol{\sigma}$ are derived.

The Helmholtz free energy per unit volume ϕ for the whole system V usually depends on the volume density of elastic energy. As it will be further shown due to the singularity of discrete plastic sources, the free energy must also include the dislocation core energy owing to elastic but non-linear core effects. Other contributions such as the stacking fault energy are neglected. Then:

$$\phi(\mathbf{E}, \boldsymbol{\epsilon}^*(\mathbf{x})) = \frac{1}{V}\int_V w_{el}\, dV, \tag{17}$$

where $\boldsymbol{\epsilon}^*(\mathbf{x})$ is the plastic strain field and $w_{el} = \frac{1}{2}\boldsymbol{\sigma}(\mathbf{x}) : \boldsymbol{\epsilon}^e(\mathbf{x})$ is the volume density of elastic energy. Eq. (17) only holds in the case of isothermal and quasi-static conditions. Following Appendix A, we demonstrate that ϕ takes the form of:

$$\phi(\mathbf{E},\boldsymbol{\epsilon}^*(\mathbf{x})) = \frac{1}{2}(\mathbf{E}-\mathbf{E}^*):\mathbf{C}:(\mathbf{E}-\mathbf{E}^*) - \frac{1}{2V}\int_V \boldsymbol{\tau}(\mathbf{x}):\boldsymbol{\epsilon}^*(\mathbf{x})\,dV, \tag{18}$$

where $\mathbf{E}^* = \frac{1}{V}\int_V \boldsymbol{\epsilon}^*(\mathbf{x})\,dV$ denotes the averaged plastic strain over the whole volume V. The last part of ϕ that contains the internal stress field $\boldsymbol{\tau}(\mathbf{x})$ will be denoted ϕ_{int} for the internal elastic energy per unit volume. Thus, the internal elastic energy named $\Phi_{\text{int}} = V \cdot \phi_{\text{int}}$ reads:

$$\Phi_{\text{int}} = -\frac{1}{2}\int_V \boldsymbol{\tau}(\mathbf{x}):\boldsymbol{\epsilon}^*(\mathbf{x})\,dV. \tag{19}$$

The internal stress $\boldsymbol{\tau}(\mathbf{x})$ is defined as follows:

$$\boldsymbol{\tau}(\mathbf{x}) = \boldsymbol{\sigma}(\mathbf{x}) - \boldsymbol{\Sigma}, \tag{20}$$

where $\boldsymbol{\Sigma}$ is the macroscopic stress defined by $\boldsymbol{\Sigma} = \frac{1}{V}\int_V \boldsymbol{\sigma}(\mathbf{x})\,dV$ and verifying the macroscopic behavior law:

$$\boldsymbol{\Sigma} = \mathbf{C}:(\mathbf{E}-\mathbf{E}^*). \tag{21}$$

In order to solve the field equations described for a non-uniform plastic field in the grain V_g, different techniques such as the method based on Green functions or numerical procedures based on spatial discretizations of plastic fields can be adopted. In the present paper, a Fourier transform method is developed. This is the object of Section 3. First of all, we recall the Eshelby's method and solutions in the case of uniform plastic field in the grain.

2.3. Eshelby's method and solutions

The Eshelby's method assumes that the plastic fields in the interior of the grain V_g considered as an inclusion reduces to a uniform plastic strain (or uniform *eigenstrain*). For exterior points to the grain, there is no plastic strain. Thus:

$$\boldsymbol{\epsilon}^*(\mathbf{x}) = \begin{cases} \boldsymbol{\epsilon}^0 & \text{for } \mathbf{x} \text{ in } V_g \\ \mathbf{0} & \text{for } \mathbf{x} \text{ outside } V_g, \end{cases} \tag{22}$$

where $\boldsymbol{\epsilon}^0$ is the uniform plastic strain. Then, in his well-known contribution, Eshelby (1957) proved that if the grain is represented by an ellipsoidal inclusion, the total strain $\boldsymbol{\epsilon}(\mathbf{x})$ remains uniform in the inclusion and does not depend on the position $\mathbf{x}$. In a second paper, Eshelby (1959) proved that the previous remarkable property does not hold for exterior points to the inclusion. From these findings, the interior and exterior solutions are:

$$\boldsymbol{\epsilon}(\mathbf{x}) = \mathbf{E} + \mathbf{S}^{E}(\mathbf{x}):\boldsymbol{\epsilon}^0, \tag{23}$$

with $\mathbf{S}^{E}(\mathbf{x})$ being the fourth order elastic Eshelby tensor which is uniform for interior points (denoted $\mathbf{S}^{E\ i}$) and non-uniform elsewhere (denoted $\mathbf{S}^{E\ e}(\mathbf{x})$). Using the Hooke's law and the previous equation allows us to derive the stress field $\boldsymbol{\sigma}(\mathbf{x})$.

In the particular case of a spherical inclusion of radius R, and, assuming isotropic elasticity for which the elastic moduli $\mathbf{C}$ write as a function of shear modulus μ and Poisson's ratio ν as:

$$C_{ijkl} = \frac{2\mu\nu}{1-2\nu}\delta_{ij}\delta_{kl} + \mu(\delta_{ik}\delta_{jl} + \delta_{il}\delta_{jk}), \tag{24}$$

the interior solution $\mathbf{S}^{E\ i}$ only depends on Poisson's ratio (Mura, 1987). Its expression in indicial notation reads:

$$S^{E\ i}_{ijkl} = \frac{5\nu-1}{15(1-\nu)}\delta_{ij}\delta_{kl} + \frac{4-5\nu}{15(1-\nu)}(\delta_{ik}\delta_{jl} + \delta_{il}\delta_{jk}), \tag{25}$$

and, the exterior solution $\mathbf{S}^{E\ e}(\mathbf{x})$ depends on the unit position vector $\overline{\mathbf{x}} = \mathbf{x}/x$ with $x = \sqrt{\mathbf{x}\cdot\mathbf{x}}$. Following Ju and Sun (1999), its expression remains analytical:

$$\begin{aligned} S^{E\ e}_{ijkl}(\mathbf{x}) = \frac{\kappa^3}{30(1-\nu)}\big[&(3\kappa^2+10\nu-5)\delta_{ij}\delta_{kl} + (3\kappa^2-10\nu+5)(\delta_{ik}\delta_{jl}+\delta_{il}\delta_{jk}) + 15(1-\kappa^2)\delta_{ij}\overline{x}_k\overline{x}_l + 15(1-2\nu-\kappa^2)\delta_{kl}\overline{x}_i\overline{x}_j \\ &+ 15(\nu-\kappa^2)(\delta_{ik}\overline{x}_j\overline{x}_l + \delta_{jk}\overline{x}_i\overline{x}_l + \delta_{il}\overline{x}_j\overline{x}_k + \delta_{jl}\overline{x}_i\overline{x}_k) + 15(7\kappa^2-5)\overline{x}_i\overline{x}_j\overline{x}_k\overline{x}_l\big], \end{aligned} \tag{26}$$

where $\kappa = R/x$.

As a consequence of the uniform Eshelby tensor inside V_g, the Eshelby's solution for Helmholtz free energy per unit volume ϕ simply yields:

$$\phi(\mathbf{E},\boldsymbol{\epsilon}^*(\mathbf{x})) = \frac{1}{2}(\mathbf{E}-\mathbf{E}^*):\mathbf{C}:(\mathbf{E}-\mathbf{E}^*) + \frac{1}{2}\frac{V_g}{V}\boldsymbol{\epsilon}^0:\mathbf{C}:(\mathbf{I}-\mathbf{S}^{E\ i}):\boldsymbol{\epsilon}^0. \tag{27}$$

The corresponding uniform internal stress inside V_g denoted $\boldsymbol{\tau}^0$ reads:

$$\boldsymbol{\tau}^0 = -\mathbf{C}:(\mathbf{I}-\mathbf{S}^{E\ i}):\boldsymbol{\epsilon}^0, \tag{28}$$

with the unit tensor $\mathbf{I}$ where $I_{ijkl} = \frac{1}{2}(\delta_{ik}\delta_{jl}+\delta_{il}\delta_{jk})$ in indicial notation. The previous formulae associated with Eshelby's solutions constitute the starting points of the equivalent inclusion method for composites or the self-consistent procedure detailed in Mura (1987) or in Nemat-Nasser and Hori (1993).

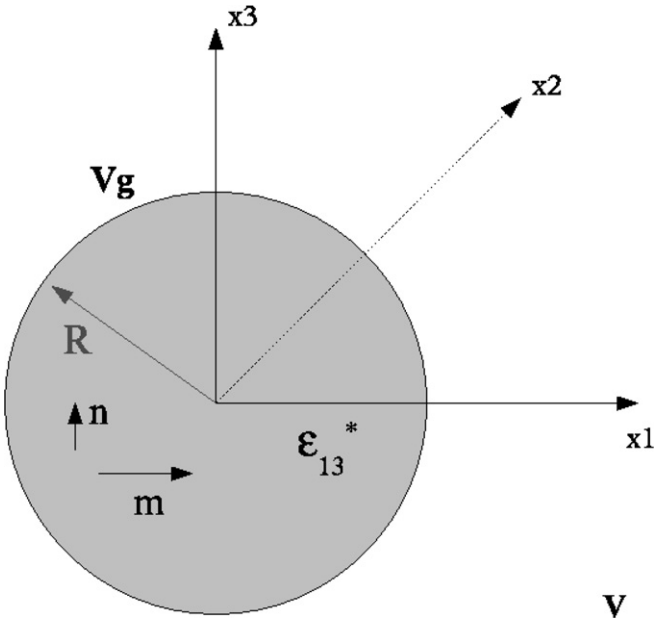

Fig. 2. Spherical grain of radius R with a uniform plastic strain ϵ^0_{13} in the sense of the Eshelby's method. The grain is embedded in an infinite elastic medium.

Let us consider now an application example of this method. Following Fig. 2, we consider a spherical grain of radius R embedded in an infinite medium V where no macroscopic strain is imposed on its boundary ∂V. Furthermore, only one single slip system is considered and characterized by the unit vector normal to the slip plane $\mathbf{n} = (0,0,1)$ and the unit vector along the slip direction $\mathbf{m} = (1,0,0)$. Then, the only non-zero plastic strain components are shear components $\epsilon^*_{13}(\mathbf{x}) = \epsilon^*_{31}(\mathbf{x}) = \frac{1}{2}\beta^*_{31}(\mathbf{x})$ defined as:

$$\epsilon^*_{13}(\mathbf{x}) = \begin{cases} \epsilon^0_{13} & \text{if } r \leqslant R \\ 0 & \text{if } r > R, \end{cases} \tag{29}$$

where $\epsilon^0_{13} = 1/2\gamma$. In this mean-field representation, γ constitutes a *uniform* plastic shear produced by glide dislocation loops *continuously* and *uniformly* distributed inside the grain. Regarding internal stress for interior points to the grain, the only non-zero component τ^0_{13} is then uniform and depends on ϵ^0_{13} and elastic constants. It comes directly from Eq. (28) that:

$$\tau^0_{13} = -2\mu \frac{7-5\nu}{15(1-\nu)} \epsilon^0_{13}. \tag{30}$$

For exterior points to the grain, the internal stress is no more uniform and for the case of the sphere, its expression is computed using Eq. (26).

In this representation, the internal elastic energy named Φ^0_{int} simply yields after Eq. (27):

$$\Phi^0_{\text{int}} = 8\mu\pi R^3 \frac{7-5\nu}{45(1-\nu)} (\epsilon^0_{13})^2. \tag{31}$$

The *mean-field* model of plastic source due to dislocation loops consists in a uniform plastic strain inside the grain for which the internal stress field and the internal elastic energy are related to the classic Eshelby tensor for a spherical inclusion. In the next sections, we will employ the Fourier transform method to derive the internal stress field and the internal elastic energy of different distributions of *dislocation loops*.

3. Fourier transform method

3.1. Mechanical fields and energy

The displacement field inside V can be decomposed into the displacement from the remote boundary load $\mathbf{u}^{\text{d}}$ and an internal (or disturbed) displacement $\mathbf{u}(\mathbf{x})$. In the following, we only focus on the internal field $\mathbf{u}(\mathbf{x})$ due to the disturbance enhanced by plastic sources in the medium.

Solving the equilibrium equation by introducing both the constitutive equation and the strain compatibility relation gives at any position $\mathbf{x}$:

$$\begin{aligned} &C_{ijkl}u_{k,lj}(\mathbf{x}) - C_{ijkl}\beta^*_{lk,j}(\mathbf{x}) = 0 \\ &u^{\mathrm{d}}_i(\mathbf{x}) = 0 \quad \text{on} \qquad \partial V. \end{aligned} \tag{32}$$

Following Mura (1987), the problem can be solved using the Fourier transform method, where displacement field $\mathbf{u}$ or distortion field $\boldsymbol{\beta}$ are solved in the Fourier space and then in the real space using the inverse Fourier transform theorem. Let $\boldsymbol{\xi}$ be the Fourier vector of magnitude $\xi = \sqrt{\boldsymbol{\xi}\cdot\boldsymbol{\xi}}$ and of components ξ_i in cartesian coordinates. We denote i as $\mathrm{i} = \sqrt{-1}$.

Let $\widetilde{u_k}(\boldsymbol{\xi})$ and $\widetilde{\beta^*_{lk}}(\boldsymbol{\xi})$ be the Fourier transforms of the displacement and the plastic distortion defined by:

$$\begin{aligned} \widetilde{u_k}(\boldsymbol{\xi}) &= \int_V u_k(\mathbf{x})\mathrm{e}^{-\mathrm{i}\boldsymbol{\xi}\cdot\mathbf{x}}\,\mathrm{d}V, \\ \widetilde{\beta^*_{lk}}(\boldsymbol{\xi}) &= \int_V \beta^*_{lk}(\mathbf{x})\mathrm{e}^{-\mathrm{i}\boldsymbol{\xi}\cdot\mathbf{x}}\,\mathrm{d}V. \end{aligned} \tag{33}$$

Conversely, the inverse Fourier transforms are defined as:

$$\begin{aligned} u_k(\mathbf{x}) &= \frac{1}{8\pi^3}\int_{V_\xi} \widetilde{u_k}(\boldsymbol{\xi})\mathrm{e}^{+\mathrm{i}\boldsymbol{\xi}\cdot\mathbf{x}}\,\mathrm{d}V_\xi, \\ \beta^*_{lk}(\mathbf{x}) &= \frac{1}{8\pi^3}\int_{V_\xi} \widetilde{\beta^*_{lk}}(\boldsymbol{\xi})\mathrm{e}^{+\mathrm{i}\boldsymbol{\xi}\cdot\mathbf{x}}\,\mathrm{d}V_\xi. \end{aligned} \tag{34}$$

Then transforming Eq. (32) in the Fourier space gives the following algebric equation to solve:

$$C_{ijkl}\xi_l\xi_j\widetilde{u_k}(\boldsymbol{\xi}) = -\mathrm{i}C_{ijkl}\xi_j\widetilde{\beta^*_{lk}}(\boldsymbol{\xi}), \tag{35}$$

or in the more compact form:

$$\widetilde{u_k}(\boldsymbol{\xi}) = \widetilde{G_{ik}}(\boldsymbol{\xi})\widetilde{X}_i(\boldsymbol{\xi}), \tag{36}$$

where $\widetilde{G_{ik}}(\boldsymbol{\xi}) = (C_{ijkl}\xi_l\xi_j)^{-1}$ and $\widetilde{X}_i(\boldsymbol{\xi})$ is defined as:

$$\widetilde{X}_i(\boldsymbol{\xi}) = -\mathrm{i}C_{ijmn}\xi_j\widetilde{\beta^*_{nm}}(\boldsymbol{\xi}). \tag{37}$$

$\widetilde{G_{ik}}(\boldsymbol{\xi})$ can be identified as the Fourier transform of the elastic Green tensor (Mura, 1987). Then, the problem solutions in the general case write:

$$\begin{aligned} u_k(\mathbf{x}) &= \frac{-\mathrm{i}}{8\pi^3}\int_{V_\xi} \xi_j C_{ijmn}\widetilde{G_{ik}}(\boldsymbol{\xi})\widetilde{\beta^*_{nm}}(\boldsymbol{\xi})\mathrm{e}^{+\mathrm{i}\boldsymbol{\xi}\cdot\mathbf{x}}\,\mathrm{d}V_\xi, \\ \beta_{lk}(\mathbf{x}) &= \frac{1}{8\pi^3}\int_{V_\xi} \xi_l\xi_j C_{ijmn}\widetilde{G_{ik}}(\boldsymbol{\xi})\widetilde{\beta^*_{nm}}(\boldsymbol{\xi})\mathrm{e}^{+\mathrm{i}\boldsymbol{\xi}\cdot\mathbf{x}}\,\mathrm{d}V_\xi. \end{aligned} \tag{38}$$

Assuming isotropic elasticity defined by shear modulus μ and Poisson's ratio ν, $\widetilde{\mathbf{G}}$ and $\widetilde{\mathbf{X}}$ read:

$$\widetilde{G_{ik}}(\boldsymbol{\xi}) = \frac{1}{\mu}\left(\frac{\delta_{ik}}{\xi^2} - \frac{1}{2(1-\nu)}\frac{\xi_i\xi_k}{\xi^4}\right), \tag{39}$$

$$\widetilde{X}_i(\boldsymbol{\xi}) = -\mathrm{i}2\mu\xi_j\left(\widetilde{\epsilon^*_{ij}}(\boldsymbol{\xi}) + \frac{\nu}{1-2\nu}\delta_{ij}\widetilde{\epsilon^*_{kk}}(\boldsymbol{\xi})\right). \tag{40}$$

Then, regarding isotropic elasticity the problem solutions for displacement and distortion fields write:

$$\begin{aligned} u_k(\mathbf{x}) &= \frac{-\mathrm{i}}{4\pi^3}\int_{V_\xi}\left(\frac{\delta_{ik}\xi_j}{\xi^2} - \frac{1}{2(1-\nu)}\frac{\xi_i\xi_j\xi_k}{\xi^4}\right)\left(\widetilde{\epsilon^*_{ij}}(\boldsymbol{\xi}) + \frac{\nu}{1-2\nu}\delta_{ij}\widetilde{\epsilon^*_{qq}}(\boldsymbol{\xi})\right)\mathrm{e}^{+\mathrm{i}\boldsymbol{\xi}\cdot\mathbf{x}}\,\mathrm{d}V_\xi, \\ \beta_{lk}(\mathbf{x}) &= \frac{1}{4\pi^3}\int_{V_\xi}\left(\frac{\delta_{ik}\xi_j\xi_l}{\xi^2} - \frac{1}{2(1-\nu)}\frac{\xi_i\xi_j\xi_k\xi_l}{\xi^4}\right)\left(\widetilde{\epsilon^*_{ij}}(\boldsymbol{\xi}) + \frac{\nu}{1-2\nu}\delta_{ij}\widetilde{\epsilon^*_{qq}}(\boldsymbol{\xi})\right)\mathrm{e}^{+\mathrm{i}\boldsymbol{\xi}\cdot\mathbf{x}}\,\mathrm{d}V_\xi. \end{aligned} \tag{41}$$

In the peculiar case where $\beta^*_{qq} = 0$ (plastic incompressibility) then Eq. (41) reduces to:

$$\begin{aligned} u_k(\mathbf{x}) &= \frac{-\mathrm{i}}{4\pi^3}\int_{V_\xi}\left(\frac{\delta_{ik}\xi_j}{\xi^2} - \frac{1}{2(1-\nu)}\frac{\xi_i\xi_j\xi_k}{\xi^4}\right)\widetilde{\epsilon^*_{ij}}(\boldsymbol{\xi})\mathrm{e}^{+\mathrm{i}\boldsymbol{\xi}\cdot\mathbf{x}}\,\mathrm{d}V_\xi, \\ \beta_{lk}(\mathbf{x}) &= \frac{1}{4\pi^3}\int_{V_\xi}\left(\frac{\delta_{ik}\xi_j\xi_l}{\xi^2} - \frac{1}{2(1-\nu)}\frac{\xi_i\xi_j\xi_k\xi_l}{\xi^4}\right)\widetilde{\epsilon^*_{ij}}(\boldsymbol{\xi})\mathrm{e}^{+\mathrm{i}\boldsymbol{\xi}\cdot\mathbf{x}}\,\mathrm{d}V_\xi. \end{aligned} \tag{42}$$

The internal stress field $\boldsymbol{\tau}(\mathbf{x})$ is derived from the Hooke's law:

$$\tau_{kl}(\mathbf{x}) = 2\mu\left(\epsilon_{kl}(\mathbf{x}) - \epsilon^*_{kl}(\mathbf{x}) + \frac{\nu}{1-2\nu}\delta_{kl}\epsilon_{qq}(\mathbf{x})\right). \tag{43}$$

Applying Parseval's identity to the last term of Eq. (18) containing internal stresses named ϕ_{int} allows us to compute it as:

$$\phi_{\mathrm{int}} = -\frac{1}{2V}\int_V \tau_{kl}(\mathbf{x})\epsilon^*_{kl}(\mathbf{x})\,\mathrm{d}V = -\frac{1}{8\pi^3}\frac{1}{2V}\int_{V_\xi}\widetilde{\tau_{kl}}(\boldsymbol{\xi})\widetilde{\epsilon^{*\star}_{kl}}(\boldsymbol{\xi})\,\mathrm{d}V_\xi, \tag{44}$$

where $\widetilde{\epsilon^{\star}_{kl}}(\boldsymbol{\xi})$ is the complex conjugate of $\widetilde{\epsilon^{*}_{kl}}(\boldsymbol{\xi})$ and $\widetilde{\tau_{kl}}(\boldsymbol{\xi})$ is the Fourier transform of $\tau_{kl}(\mathbf{x})$. This one can be computed as follows:

$$\widetilde{\tau_{kl}}(\boldsymbol{\xi}) = 2\mu\Big(\widetilde{\epsilon_{kl}}(\boldsymbol{\xi}) - \widetilde{\epsilon^{*}_{kl}}(\boldsymbol{\xi}) + \frac{\nu}{1-2\nu}\delta_{kl}\widetilde{\epsilon_{qq}}(\boldsymbol{\xi})\Big), \tag{45}$$

with $\widetilde{\epsilon_{kl}}(\boldsymbol{\xi}) = \frac{1}{2}\mathrm{i}(\xi_l\widetilde{G_{ik}}(\boldsymbol{\xi}) + \xi_k\widetilde{G_{il}}(\boldsymbol{\xi}))\widetilde{X_i}(\boldsymbol{\xi})$.

The methodology to determine the whole mechanical fields and elastic energy is the following. The first step is to compute the Fourier transforms of plastic distortion and plastic strain (i.e. the *eigenstrain*). Then, in order to calculate the displacement $\mathbf{u}(\mathbf{x})$ the integration is performed in the Fourier space. The total strain $\boldsymbol{\epsilon}(\mathbf{x})$ can be computed either from the displacement in the real space or in the Fourier space. Then, the internal stress $\boldsymbol{\tau}(\mathbf{x})$ is computed in the real space using the Hooke's law. Following Eq. (45), we also use the stress field in the Fourier space to obtain the internal elastic energy $\Phi_{\mathrm{int}} = V \cdot \phi_{\mathrm{int}}$ from Parseval's identity. The main difficulties arise from the calculation of $\widetilde{\boldsymbol{\beta}^{*}}(\boldsymbol{\xi})$ and from the mathematical integrations. We give in the next section different situations for which the calculations are explicited to derive internal stresses and internal elastic energies.

4. Applications

4.1. Case of 1 circular glide loop

Let us first consider the case of one circular glide loop of radius a lying in the plane $(x_1, x_2, 0)$ and centered at the origin (Fig. 3). The loop is characterized by its Burgers vector $\mathbf{b}$ defined in the direction x_1 by $\mathbf{b} = (b, 0, 0)$ and by its unit normal to the glide plane $\mathbf{n} = (0, 0, 1)$. Applying Eq. (2) to the present application, the only non-zero component for the plastic distortion due to the loop is:

$$\beta^{*}_{31}(\mathbf{x}) = bH\Big(1 - \frac{\rho}{a}\Big)\delta(x_3) = b\theta^{1\mathrm{d}}(\mathbf{x}), \tag{46}$$

where ρ and x_3 denote, respectively, the radial coordinate and the altitude in cylindrical coordinates (ρ, θ, x_3) defined as $(x_1 = \rho\cos\theta, x_2 = \rho\sin\theta, x_3)$. In the previous equation, $\theta^{1\mathrm{d}}(\mathbf{x})$ is the characteristic function of the disc of radius a (superscript 1d denotes *one dislocation loop*), $\delta(x_3)$ is the one-dimensional Dirac delta function in the direction (x_3) and H is the Heaviside step function such that:

$$H\Big(1 - \frac{\rho}{a}\Big) = \begin{cases} 1 & \text{if } \rho \leqslant a \\ 0 & \text{if } \rho > a. \end{cases} \tag{47}$$

The Fourier transform of the plastic distortion is obtained after a few calculations using Eq. (33) and the Fourier transform $\theta^{1\mathrm{d}}(\boldsymbol{\xi})$ of $\theta^{1\mathrm{d}}(\mathbf{x})$ such that:

$$\widetilde{\beta^{*}_{31}}(\boldsymbol{\xi}) = b\widetilde{\theta^{1\mathrm{d}}}(\boldsymbol{\xi}) = b\int_0^a\int_0^{2\pi} \mathrm{e}^{-\mathrm{i}q\rho\cos(\theta-\phi)}\rho\,\mathrm{d}\rho\,\mathrm{d}\theta = 2\pi ba\frac{J_1(aq)}{q}, \tag{48}$$

where J_1 is the Bessel function of first kind. ξ_1 and ξ_2 can write $\xi_1 = q\cos\phi$, $\xi_2 = q\sin\phi$, with $q = \sqrt{\xi_1^2 + \xi_2^2}$. Using Eq. (42), we find in the peculiar representation of Fig. 3 that:

$$\begin{aligned} u_k(\mathbf{x}) &= \frac{-\mathrm{i}}{4\pi^3}\int_{V_\xi}\left(\frac{\delta_{1k}\xi_3 + \delta_{3k}\xi_1}{\xi^2} - \frac{1}{1-\nu}\frac{\xi_1\xi_3\xi_k}{\xi^4}\right)\widetilde{\epsilon^{*}_{13}}(\boldsymbol{\xi})\mathrm{e}^{+\mathrm{i}\boldsymbol{\xi}\mathbf{x}}\,\mathrm{d}V_\xi, \\ \epsilon_{kl}(\mathbf{x}) &= \frac{1}{8\pi^3}\int_{V_\xi}\left(\frac{\delta_{1k}\xi_3\xi_l + \delta_{1l}\xi_3\xi_k + \delta_{3k}\xi_1\xi_l + \delta_{3l}\xi_1\xi_k}{\xi^2} - \frac{2}{1-\nu}\frac{\xi_1\xi_3\xi_k\xi_l}{\xi^4}\right)\widetilde{\epsilon^{*}_{13}}(\boldsymbol{\xi})\mathrm{e}^{+\mathrm{i}\boldsymbol{\xi}\mathbf{x}}\,\mathrm{d}V_\xi. \end{aligned} \tag{49}$$

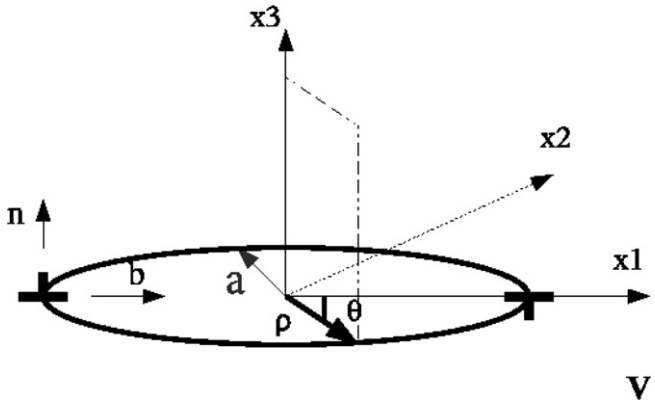

Fig. 3. Definition of a centered circular glide loop of radius a of unit normal $\mathbf{n}$ and of Burgers $\mathbf{b}$ in cylindrical and cartesian coordinates.

The internal stress field due to the loop is derived from the Hooke's law in isotropic elasticity and its components are calculated in cylindrical coordinates after derivations making use of the Lipschitz–Hankel type integrals involving products of Bessel functions (see Appendix B). Their final expressions depending on ρ, θ and x_3 write:

$$\begin{aligned}
\tau_{11}(\mathbf{x}) &= \frac{\mu b}{2(1-\nu)}\cos\theta \mathrm{sgn}(x_3)\left\{-\frac{2}{a}J(1,1;1)+\frac{|x_3|}{a^2}\left(\cos^2\theta J(1,1;2)+\frac{a}{\rho}(3-4\cos^2\theta)J(1,2;1)\right)\right\}\\
\tau_{13}(\mathbf{x}) &= \frac{\mu b}{2(1-\nu)}\left\{\frac{\nu-1-\nu*\cos^2\theta}{a}J(1,0;1)+\frac{\nu}{\rho}\cos 2\theta J(1,1;0)+\frac{|x_3|}{a^2}\left(\cos^2\theta J(1,0;2)-\frac{a}{\rho}\cos 2\theta J(1,1;1)\right)\right\}\\
\tau_{12}(\mathbf{x}) &= \frac{\mu b}{2(1-\nu)}\sin\theta \mathrm{sgn}(x_3)\left\{-\frac{1-\nu}{a}J(1,1;1)+\frac{|x_3|}{a^2}\left(\cos^2\theta J(1,1;2)-\frac{a}{\rho}(3-4\sin^2\theta)J(1,2;1)\right)\right\}\\
\tau_{22}(\mathbf{x}) &= \frac{\mu b}{2(1-\nu)}\cos\theta \mathrm{sgn}(x_3)\left\{-\frac{2\nu}{a}J(1,1;1)+\frac{|x_3|}{a^2}\left(\sin^2\theta J(1,1;2)-\frac{a}{\rho}(3-4\cos^2\theta)J(1,2;1)\right)\right\}\\
\tau_{23}(\mathbf{x}) &= \frac{\mu b}{4(1-\nu)}\sin 2\theta\left\{\frac{\nu}{a}J(1,2;1)-\frac{|x_3|}{a^2}J(1,2;2)\right\}\\
\tau_{33}(\mathbf{x}) &= -\frac{\mu b}{2(1-\nu)}\cos\theta\frac{x_3}{a^2}J(1,1;2).
\end{aligned} \tag{50}$$

In the previous expressions, $\mathrm{sgn}(x_3)=+1$ for $x_3>0$ and $\mathrm{sgn}(x_3)=-1$ for $x_3<0$. $J(m,n;p)$ where m, n and p are integers are Lipschitz–Hankel integrals (Eason et al., 1955; Salamon and Walter, 1979). They are defined by $J(m,n;p)=\int_0^{+\infty}J_m(Q)J_n(\overline{\rho}Q)\mathrm{e}^{-\frac{Q|x_3|}{a}}Q^p\,\mathrm{d}Q$ with $\overline{\rho}=\rho/a$, $Q=a\sqrt{\xi_1^2+\xi_2^2}$ and $J_m(Q)$ are Bessel functions of integer order m. The last expressions are then numerically computed in the form of complete elliptic integrals of first kind $\mathbf{K}(k)$ and second kind $\mathbf{E}(k)$ where the modulus k is explicited in Appendix B.

The internal elastic energy of one single circular glide dislocation loop has been computed independently using the Parseval's identity for $\Phi_{\mathrm{int}}=V\cdot\phi_{\mathrm{int}}$ according to Eq. (44) denoted $\Phi_{\mathrm{int}}^{1\mathrm{d}}$:

$$\Phi_{\mathrm{int}}^{1\mathrm{d}}=\frac{\mu b^2}{16\pi^3}\int_{V_\xi}\left(\frac{\xi_2^2}{\xi^2}+\frac{2}{1-\nu}\frac{\xi_1^2\xi_3^2}{\xi^4}\right)\mid\widetilde{\theta^{1\mathrm{d}}}(\boldsymbol{\xi})\mid^2\mathrm{d}V_\xi, \tag{51}$$

with $\mid\widetilde{\theta^{1\mathrm{d}}}(\boldsymbol{\xi})\mid^2=4\pi^2a^2(J_1(aq))^2/q^2$ from Eq. (48).

Here, the difficulty arises from the mathematical integration in the last equation. Due to the dislocation core region where linear elastic properties fail (singularity of the stress field), a convenient way to do it is to calculate the energy of one dislocation loop as half the interaction energy between two identical circular dislocation glide loops separated by a distance $2r_c$ (Hirth and Lothe, 1982). This cut-off distance can be identified as the *core radius* which is here an *ad-hoc parameter*. The mathematical integration to give the interaction energy is reported in Appendix B. Then, the final expression of the elastic energy of a single loop (also called self-energy) contains complete elliptic integrals of first and second kinds, respectively $\mathbf{K}(k)$ and $\mathbf{E}(k)$, according to:

$$\Phi_{\mathrm{int}}^{1\mathrm{d}}=\frac{\mu b^2}{2}a\frac{2-\nu}{1-\nu}\frac{1}{k}\left(\left(1-\frac{k^2}{2}\right)\mathbf{K}(k)-\mathbf{E}(k)\right), \tag{52}$$

with:

$$k^2=\frac{a^2}{a^2+r_c^2}. \tag{53}$$

4.2. Distribution of periodic glide dislocation loops along one direction

Now, we focus the study on a distribution of periodic circular glide dislocation loops lying in successive planes parallel to $(x_1,x_2,0)$ along the grain of radius R (Fig. 4). Successive loops are spaced by a given distance h. All loops are constrained by the spherical grain boundary (considered as no penetrable to dislocations) and have same Burgers vector $\mathbf{b}$ defined as $\mathbf{b}=(b,0,0)$ and same unit normal $\mathbf{n}=(0,0,1)$. The first objective is to derive the plastic distortion field for this periodic distribution. As shown in Fig. 4, an odd number $(2N+1)$ of circular loops is considered so that the only non-zero plastic distortion component is:

$$\beta_{31}^*(\mathbf{x})=b\sum_{n=-N}^{+N}H\left(1-\frac{\rho}{a^{(n)}}\right)\delta(x_3-nh), \tag{54}$$

where $a^{(n)}=\sqrt{R^2-(nh)^2}$ is the radius of the loop at altitude $x_3=nh$. After a few calculations, the Fourier transform reads:

$$\widetilde{\beta_{31}^*}(\boldsymbol{\xi})=b\widetilde{\theta^{\mathrm{d}}}(\boldsymbol{\xi}), \tag{55}$$

where:

$$\widetilde{\theta^{\mathrm{d}}}(\boldsymbol{\xi})=2\pi\sum_{n=-N}^{+N}\mathrm{e}^{-\mathrm{i}nh\xi_3}a^{(n)}\frac{J_1(a^{(n)}q)}{q}. \tag{56}$$

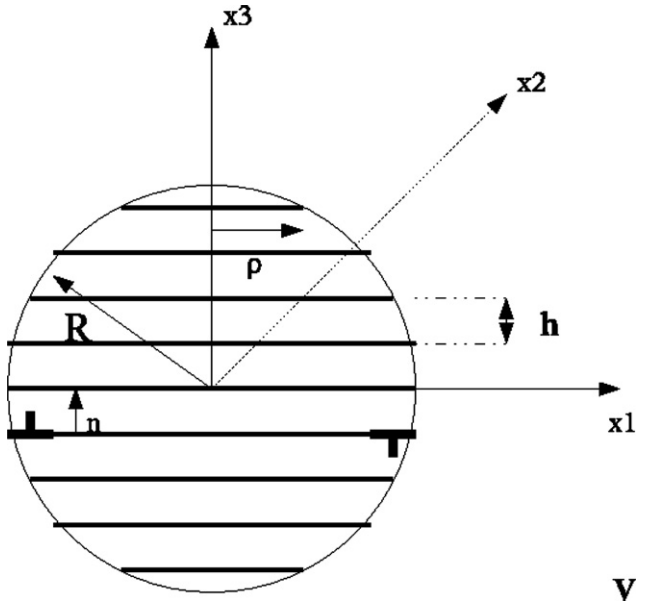

Fig. 4. Spherical grain with radius R and periodic dislocation loops spaced by h. The grain is embedded in an infinite elastic medium.

For this distribution, the averaged plastic distortion over the grain volume V_g contains the areas (denoted $S^{(n)}$) formed by the circular loops of radius $a^{(n)}$:

$$\overline{\beta_{31}^{*}}^{V_g} = b\frac{\sum_{n=-N}^{+N} S^{(n)}}{V_g} = \frac{3}{4}\frac{b}{R}\sum_{n=-N}^{+N}\left(1-\left(\frac{nh}{R}\right)^2\right). \tag{57}$$

The internal stress field is simply obtained by summing the internal stress fields off all individual circular glide loops of consecutive radii $a^{(n)}$ at altitudes $x_3 = nh$ for n varying from $-N$ to N. The peculiar case of $n = 0$ gives the internal elastic stress field of one loop centered at the origin (Eq. (50)). Thus, at any position vector $\mathbf{x}$ of altitude x_3, we compute the total internal elastic stress field as:

$$\tau_{ij}(\mathbf{x}) = \sum_{n=-N}^{+N} \tau_{ij}^{(n)}(\rho,\theta,x_3 - nh). \tag{58}$$

In Section 5, the volume density of elastic energy is also computed for isotropic elasticity:

$$w_{el}(\mathbf{x}) = \frac{1}{4\mu}\left(\tau_{ij}(\mathbf{x})^2 - \frac{\nu}{1+\nu}\tau_{qq}(\mathbf{x})^2\right). \tag{59}$$

Since the only non-zero plastic strains are again $\epsilon_{13}^{*} = \epsilon_{31}^{*} = \frac{1}{2}\beta_{31}^{*}$, we apply the Parseval's identity to find out the internal elastic energy due to the *discrete distribution of loops* denoted Φ_{int}^{d}:

$$\Phi_{int}^{d} = \frac{\mu b^2}{16\pi^3}\int_{V_\xi}\left(\frac{\xi_2^2}{\xi^2} + \frac{2}{1-\nu}\frac{\xi_1^2\xi_3^2}{\xi^4}\right)\mid\widetilde{\theta^{d}}(\boldsymbol{\xi})\mid^2 \mathrm{d}V_\xi, \tag{60}$$

with:

$$\mid\widetilde{\theta^{d}}(\boldsymbol{\xi})\mid^2 = 4\pi^2\sum_{n=-N}^{+N} a^{(n)^2}\frac{\left(J_1(a^{(n)}q)\right)^2}{q^2} + 8\pi^2\sum_{n=-N}^{N-1}\sum_{m=n+1}^{+N}\cos\left((m-n)h\xi_3\right)a^{(n)}a^{(m)}\frac{J_1(a^{(n)}q)J_1(a^{(m)}q)}{q^2}. \tag{61}$$

Thus, the elastic energy derived in Eq. (60) contains two contributions as seen in Eq. (61). The first term can be identified as the *self-energies* of the $2N+1$ dislocation loops which are derived from the expression for 1 loop (Eq. (52) or Eq. (B.7)) and the second term can be identified as the contribution of *interaction energies* between the loops which is detailed now. Considering two coaxial circular glide loops of respective radii $a^{(n)}$ and $a^{(m)}$ and separated by a distance d, we have (superscript *2*d denotes *two coaxial dislocation loops*):

$$\mid\theta^{2d}(\boldsymbol{\xi})\mid^2 = 4\pi^2\left[a^{(n)^2}\frac{(J_1(a^{(n)}q))^2}{q^2} + a^{(m)^2}\frac{(J_1(a^{(m)}q))^2}{q^2}\right] + 8\pi^2\cos(d\xi_3)a^{(n)}a^{(m)}\frac{J_1(a^{(n)}q)J_1(a^{(m)}q)}{q^2}. \tag{62}$$

Through the previous expressions, the first two terms correspond to the self-energies $\Phi_{\text{self}}^{(n)or(m)}$ of the loops with radii $a^{(n)or(m)}$ computed using Eq. (52) or Eq. (B.7). The last term represents their interaction energy $\Phi_{\text{inter}}^{(nm)}$ which writes:

$$\Phi_{\text{inter}}^{(nm)} = \frac{\mu b^2 a^{(n)} a^{(m)}}{2\pi} \int_{V_\xi} \left(\frac{\xi_2^2}{\xi^2} + \frac{2}{1-\nu} \frac{\xi_1^2 \xi_3^2}{\xi^4} \right) \cos(\mathrm{d}\xi_3) \frac{J_1(a^{(n)}q) J_1(a^{(m)}q)}{q^2} \, \mathrm{d}V_\xi. \tag{63}$$

The mathematical integration of Eq. (63) is reported in Appendix B. Its final expression yields:

$$\Phi_{\text{inter}}^{(nm)} = \mu b^2 \sqrt{a^{(n)} a^{(m)}} \frac{2-\nu}{1-\nu} \frac{1}{k} \left(\left(1 - \frac{k^2}{2} \right) \mathbf{K}(k) - \mathbf{E}(k) \right) - \frac{\mu b^2}{4} \frac{1}{\sqrt{a^{(n)} a^{(m)}}} \frac{d^2 k}{1-\nu} \left(\left(1 - \frac{k^2}{2} \right) (1-k^2)^{-1} \mathbf{E}(k) - \mathbf{K}(k) \right), \tag{64}$$

with:

$$k^2 = \frac{4 a^{(n)} a^{(m)}}{\left(a^{(n)} + a^{(m)} \right)^2 + d^2}. \tag{65}$$

Finally, by carefully summing self- and interaction-energies, we obtain the elastic energy of the discrete distribution $\Phi_{\text{int}}^{\text{d}}$ as:

$$\Phi_{\text{int}}^{\text{d}} = \sum_{n=-N}^{+N} \Phi_{\text{self}}^{(n)} + \sum_{n=-N}^{N-1} \sum_{m=n+1}^{+N} \Phi_{\text{inter}}^{(nm)}. \tag{66}$$

In Section 5, various distributions corresponding to different values of spatial period h and different grain radii R will be considered. The respective role of self- and interaction-energies on the results will be examined.

5. Results

5.1. Single circular glide loop

The internal stress field due to a single dislocation glide loop is visualized by spatial contour surfaces. For simulations, we set the Poisson's ratio to $\nu = 0.3$ and the Burgers vector to $b = 2.5 \times 10^{-10}$ m. The stress is normalized with respect to μ. As an example, we reported on Fig. 5 the normalized component τ_{13}/μ following Eq. (50) in the case of a loop of radius $a = 0.1$ μm. Fig. 5(a) and (b) represent the planar distributions of τ_{13}/μ shown as three-dimensional plots at respective altitudes of $x_3 = 0.1a$ and $x_3 = 0.5a$. The stress field for one loop was checked by comparing our results to the ones obtained by Khraishi et al. (2000) who used another method (from the integration of the Burgers equation). Like them, we checked that Eq. (50) respects the static stress equilibrium equations. Furthermore, in the limit as $a \to \infty$, it is found that the stress field of an infinite edge dislocation is retrieved in the vicinity of the points with coordinates $(a, 0, x_3)$ and $(-a, 0, x_3)$, and, that of an infinite screw dislocation is retrieved in the vicinity of the points with coordinates $(0, a, x_3)$ and $(0, -a, x_3)$. By examining the shapes of the three-dimensional surfaces at these two altitudes, a strong stress gradient is noticeable when the position vector $\mathbf{x}$ approaches the dislocation line. Moreover, the stress gradient as well as the stress amplitude is less and less pronounced as altitude x_3 is far from the plane of the loop ($x_3 = 0$). At $x_3 = 0.1a$, the maximum internal stress amplitude is one order of magnitude higher than at $x_3 = 0.5a$.

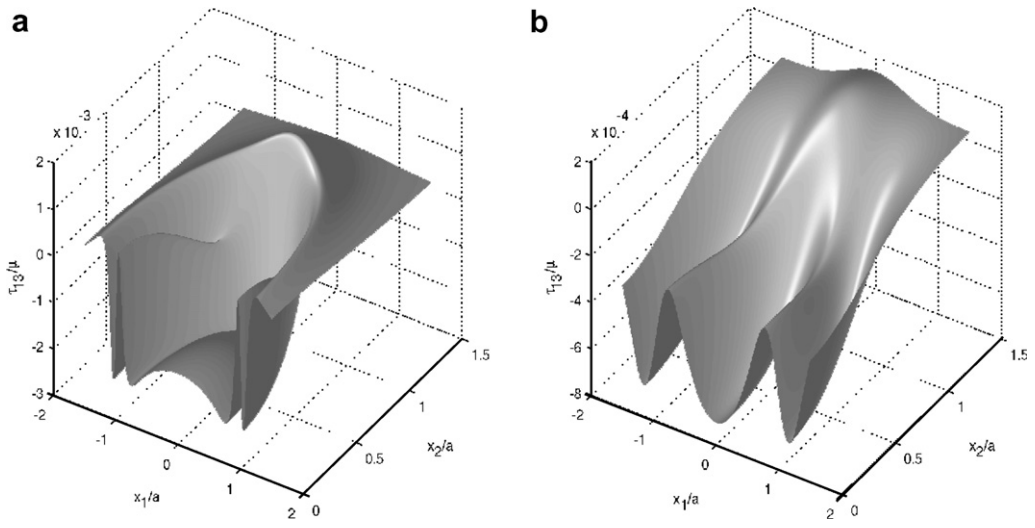

Fig. 5. Three-dimension surface plots of the normalized internal stress τ_{13}/μ due to a glide loop of radius a at altitude: (a) $x_3 = 0.1a$, (b) $x_3 = 0.5a$.

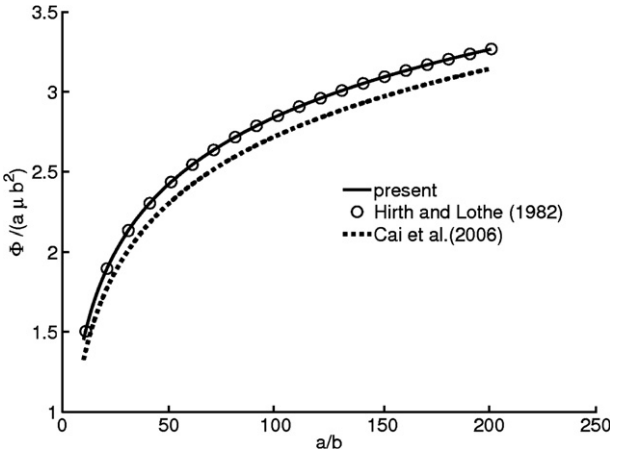

Fig. 6. Different approaches to compute the elastic energy for one circular loop (also called self-energy of the loop): present approach, formula given by Hirth and Lothe (1982), non-singular approach by Cai et al. (2006). This figure aims to show the loop size dependence of the self-energy and the relevancy of the *ad-hoc* core parameter r_c.

The normalized elastic energy $\Phi_{self}/(a\mu b^2)$ of one circular loop is plotted as a function of the loop radius a (Fig. 6). In this figure, we compared the results provided by three formulae: the first one is computed using the expression of Φ_{int}^{1d} (Eq. (52)), the second one corresponds to the formula given by Hirth and Lothe (1982, p. 169), and, the last one is the non-singular expression recently given in Cai et al. (2006). We can notice that our expression (Eq. (52)) matches the expression of Hirth and Lothe (1982) for the same value of core parameter r_c. Here, r_c is set to $0.5b$ in order to account for the contribution of the dislocation core following DeWit (1960). Both formulations correspond to the singular representation (Volterra's description) and the expression given in Hirth and Lothe (1982) is an asymptotic approximation of Eq. (52) for $r_c \ll a$. In comparison, the non-singular expression of Cai et al. (2006) assumes an isotropic dislocation core distribution by introducing a Burgers vector density function around the dislocation line. In the non-singular formulation of Cai et al. (2006), the core width parameter which is a regularization parameter is set to $1.5b$, a typical value which can be obtained through an atomistic model. A slight difference with the non-singular expression depending on the core width parameter can occur as shown on Fig. 6. However, this difference disappears when the core width parameter of Cai et al. (2006) is adjusted to $1.25b$ while r_c is kept to $0.5b$ in Eq. (53).

5.2. Periodic distribution of dislocation loops

5.2.1. Internal stress fields

Fig. 7 displays the internal stress contour in the plane (x_1,x_2) for the shear component τ_{13} at altitude $x_3 = 0.5R$ in case where different numbers of discrete dislocation loops spread in the grain (of volume V_g). By construction, the number of loops is always an odd number. Here, we respectively consider 3 loops (Fig. 7(a)), 11 loops (Fig. 7(b)) and 101 loops (Fig. 7(c)). Now, τ_{13} is normalized with $\mu\epsilon_{13}^0$ to be compared with the Eshelby's solution at same average plastic strain ϵ_{13}^0 over the grain. We can show using Eq. (50) that the ratio $\tau_{13}/\epsilon_{13}^0$ is independent of the value of the grain radius R. Hence, the result of Fig. 7 holds whatever the value of R. For comparison, Fig. 7(d) displays the case of the Eshelby's solution of uniform plastic strain ϵ_{13}^0 inside the grain. As shown in Fig. 7, it seems that the internal stresses due to a distribution of periodic loops in the (x_3) direction are almost uniform in a region surrounding the center of the sphere (named *grain core*) and are highly inhomogeneous in the remaining region close to the grain boundary (named *grain boundary layer*).

Fig. 8 displays the variation of $\tau_{13}/(\mu\epsilon_{13}^0)$ (i.e. the same shear component as on Fig. 7) along the (x_3) axis as a function of x_3/R for $\rho = 0$. Figs. 7 and 8 clearly show that a gradual increase in the number of loops inside the grain leads to a reduction of the *grain boundary layer* thickness (in the 3D space). The result given by the analytical Eshelby's solution is retrieved for a very high number of closely separated loops within the physical limit where dislocation cores do not overlap. This tendency which is observed for τ_{13} is also valid for other internal stress components as well as for the volume density of elastic energy w_{el} computed from Eq. (59).

In order to follow the evolution of the *grain boundary layer* thickness, we focus on the volume density of elastic energy w_{el}. This variable is more relevant than one single internal stress component since it accounts for all the components. Our methodology is to first assume a spherical shape for the *grain core* and to define its radius as r_a. In spherical coordinates and in one direction of the space, we record the maximum value of radial distance r for which the relative variation between w_{el} at r and w_{el} at $r = 0$ does not exceed a given value (uniformity's criterion). The value for r_a is then defined as the minimum of all the previous recorded values in all space's directions. Thus, r_a is the radius of an interior sphere where the internal stress field can be considered uniform. The thickness l of the *grain boundary layer* can then be defined as $R - r_a$. In this region, the internal stresses are highly inhomogeneous.

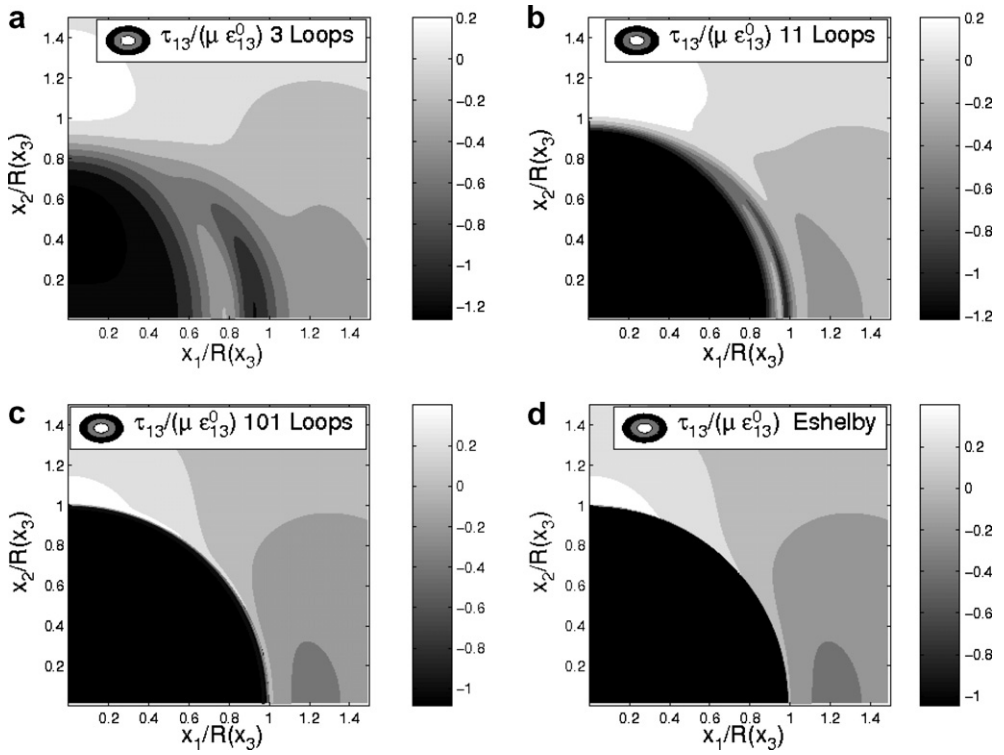

Fig. 7. Contours for internal stress component τ_{13} normalized with $\mu\epsilon^0_{13}$ at $x_3 = 0.5R$ for different number of loops. Comparison with the Eshelby's solution at same average plastic strain over the grain. (x_1, x_2) are normalized with $R(x_3) = \sqrt{R^2 + x_3^2}$.

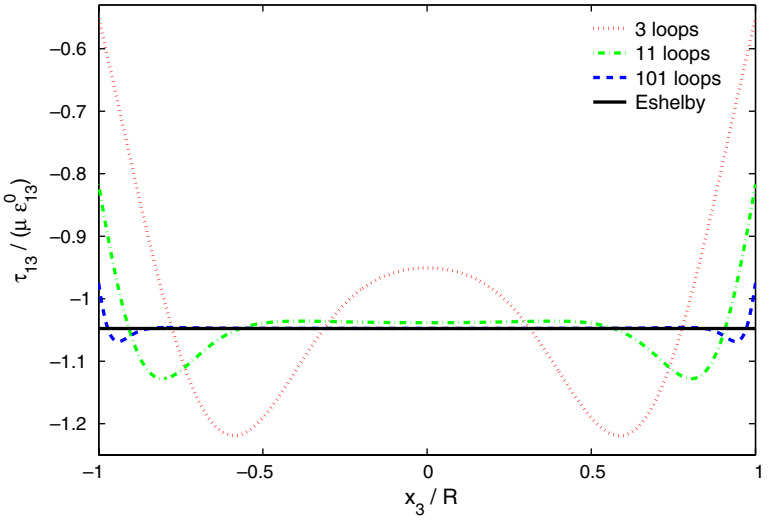

Fig. 8. Variation of the internal stress component τ_{13} normalized with $\mu\epsilon^0_{13}$ along the (x_3) axis at $\rho = 0$ for different number of loops. Comparison with the Eshelby's solution at same average plastic strain over the grain.

As an illustration, Fig. 9 represents w_{el} along three different space's directions for a given number of loops (11). This figure first shows as Figs. 7 and 8 that the Eshelby's result is retrieved in the *grain core* which here represents about 80% of the grain radius. Second, it mainly focuses on the complexity of the internal stress field inside the *grain boundary layer*. Indeed, it appears that both the maximum stress amplitude and the stress gradients depend on the space's direction which makes the description of the layer difficult. Anyway, it would be incomplete to characterize the *grain boundary layer* only by its average internal stress field and its volume fraction. On the mechanical ground, this result tackles the relevancy of composite models

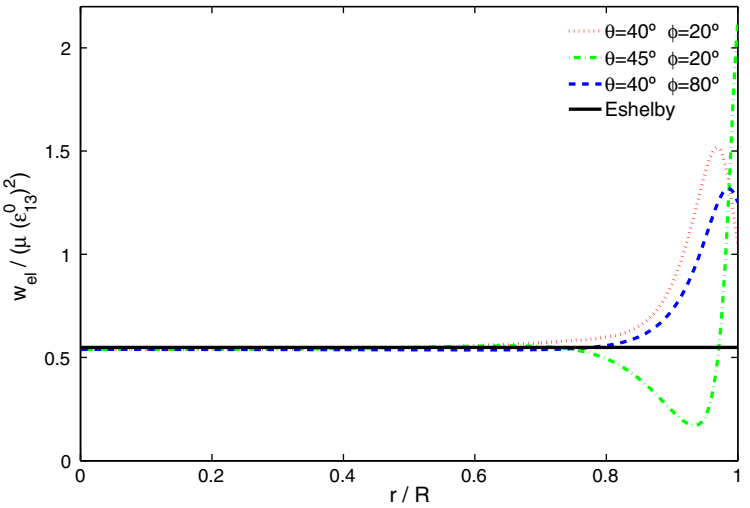

Fig. 9. Volume density of elastic energy w_{el} inside the grain along three different space's directions considering a number of 11 loops ($R/h = 5.5$). In spherical coordinates, r is the radial coordinate, and, $\theta \in (0, 180^o)$, $\phi \in (0, 360^o)$. Comparison with the Eshelby's solution at same average plastic strain over the grain.

assuming that the total internal stress follows a simple mixture rule using an average stress in the *grain core* and an average stress in the *grain boundary layer* (Margolin and Stanescu, 1975). Statistical moments of higher orders must be used to accurately quantify the internal stresses inside the boundary layer.

Fig. 10 shows the evolution of r_a and l with the number of dislocation loops according to a uniformity's criterion of 5%. It must be noticed that it is only a qualitative study as the value of 5% is arbitrary. However, the overall evolution trend remains similar for a more or less severe criterion. Actually, because of the invariance of $\tau_{13}/\epsilon^0_{13}$ with R, it is equivalent to increase the number of loops inside the grain or to increase the grain size while keeping the distance h between loops constant. For this reason, r_a and l are plotted on Fig. 10 as a function of R/h. By construction, we have $R/h = (2N+1)/2$ where $2N+1$ is the total number of loops within the grain. As expected, Fig. 10 shows that l decreases as R/h increases. The relative fast transition from a quite large to a thin *grain boundary layer* when the number of loops increases is related to the spatial distribution of loops. By construction, the loops are always equally spaced across the grain (h is constant), which leads to the most "homogeneous" possible configurations for a given number of loops. The evolutions of r_a and l (especially the transient state) would have been different in the case of non-periodic distributions of discrete loops. Only the asymptotic cases would have been similar (i.e. the case of a single loop located in the middle of the grain and the case of a very high number of loops corresponding to $R \gg h$).

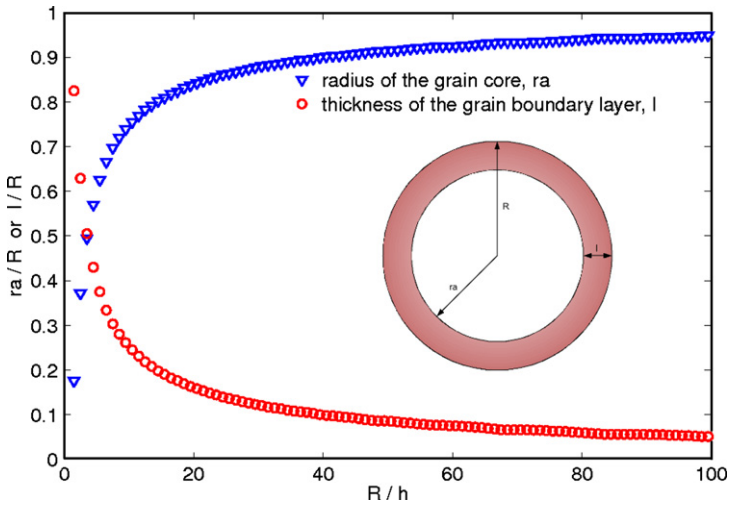

Fig. 10. Radius of the *grain core* region and thickness of the *grain boundary layer* as a function of R/h (uniformity's criterion of 5% based on w_{el}). Inset: Diagram illustrating the concept of *grain core* (white area) and *grain boundary layer* (gray area) for a spherical grain of radius R.

Fig. 11 shows that the volume density of elastic energy in the *grain core* region rapidly converges towards the Eshelby's solution. This demonstrates a rapid transition (for $R/h \sim 10$) from a regime dictated by *discrete loops* when h is on the same order than R to a regime well described by the *continuous mean-field approximation* when the separation of internal scales is clearly obtained (i.e. $h \ll R$). However, for the same reason as before, non-periodic distributions would have given slower and more complex transitions. All these results were obtained according to a uniformity's criterion based on w_{el}. Similar conclusions were found if the *grain boundary layer* was defined through a uniformity's criterion based on only one internal stress component.

5.2.2. Elastic energies

Unlike the internal stress fields, the elastic energy (once normalized with $8\mu\pi R^3(\epsilon^0_{13})^2$ to be compared with the grain size independent Eshelby's solution) is not invariant with R (Fig. 12). This effect arises from the expression of the self-energy (Eq. (52)) which accounts for the dislocation core parameter r_c in the modulus of complete elliptic integrals (Eq. (53)). As the Burgers vector is the same for each loop whatever the grain size, this variation with R is all the more important as grain size is decreased. For a periodic distribution of loops, it is seen from Fig. 12 that the normalized internal elastic energy decreases for an increasing number of loops inside the grain. The convergence towards the Eshelby's solution now depends on R. The

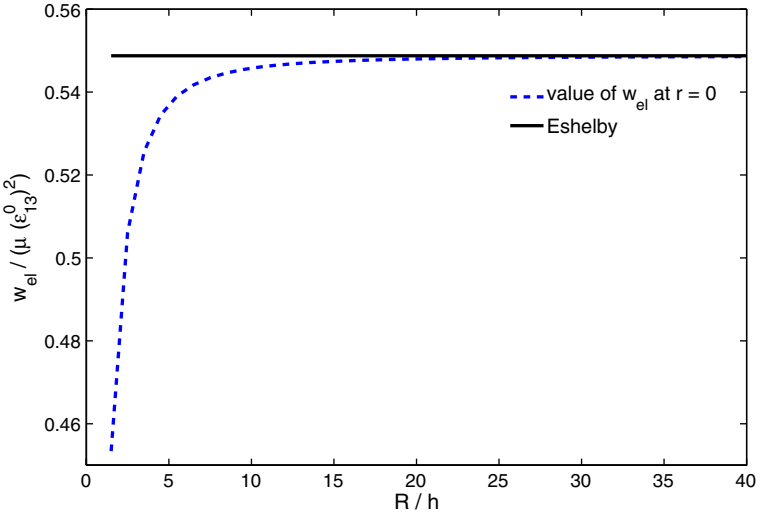

Fig. 11. Evolution of the volume density of elastic energy w_{el} in the *grain core* as a function of R/h. Comparison with the Eshelby's solution at same average plastic strain over the grain.

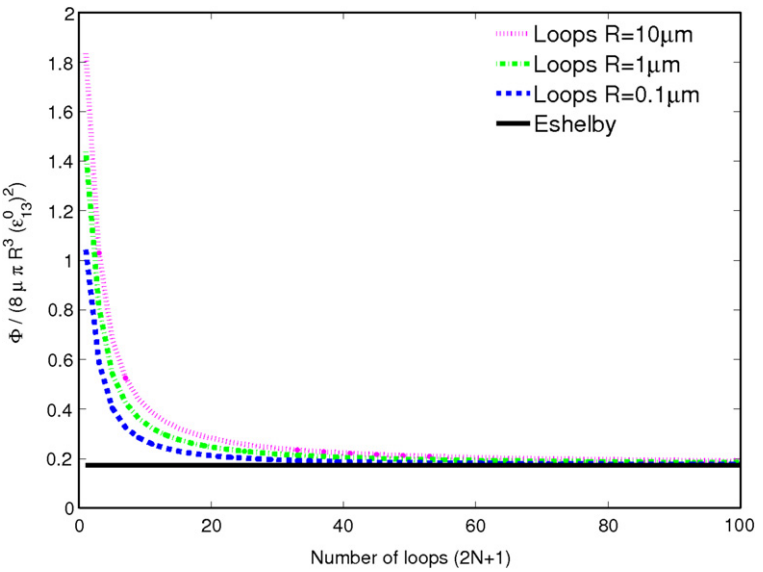

Fig. 12. Evolution of the normalized elastic energy for a periodic distribution of single glide dislocation loops as a function of the number of loops inside the grain for various grain sizes. Comparison with the Eshelby's solution at same average plastic strain over the grain.

Eshelby's solution with a uniform plastic strain ϵ^0_{13} inside the grain is actually retrieved numerically for the distance $h_{\min} \simeq 3.332b$. This value is only a numerical value which has no physical meaning as the annihilation distance between edge dipoles is found to be on the order of some tens atomic distances (Essmann and Mughrabi, 1979).

Fig. 13 displays two contributions of the internal elastic energy: the first one is due to the self-energies of dislocations loops and the second one is due to the interactions between them. This result shows that for a small number of loops, the normalized elastic energy is mainly governed by the sum of all self-energies whereas for a high number, the contribution due to pair interactions becomes predominant.

On Fig. 14, we report the evolution of the normalized elastic energy with R for constant values of mean plastic strain ϵ^0_{13} and distance h between loops. A $1/R$ scaling law is observed. This grain size effect can be written as follows:

$$\Phi^{(N)} = \alpha \frac{1}{R} + \Phi^{(N)}_{\text{Eshelby}}. \tag{67}$$

$\Phi^{(N)}$ denotes the *normalized* elastic energy. As observed on Fig. 14, the coefficient α depends on ϵ^0_{13}. Here, ϵ^0_{13} is fixed by the chosen value for h according to Eq. (57). The relation between α and ϵ^0_{13} (or h) can be easily identified using Fig. 14. Here, α decreases with h which means that the grain size effect is even less pronounced that the values of h are low. Thus, Fig. 14 demonstrates that a *microstructural error* occurs when the discrete nature of slip is neglected and when plastic slip is assumed homogeneous over the grain. The most important result lies in the grain size dependence of the elastic energy linked to the *discrete microstructure*.

5.2.3. Backstress

Now, we consider the thermodynamic driving force T defined by $T = -\partial\phi/\partial\gamma$ where ϕ is the Helmholtz free energy per unit volume (Eq. (18)), and, γ is the mean plastic slip produced by the loops over V_g (such as $\epsilon^0_{13} = 1/2\gamma$). Then, we can compute the *backstress* denoted τ^* due to plastification inside the grain. If we employ the first approach based on the Eshelby's uniform plastic inclusion, we simply find using Eq. (27) that:

$$T = f_g\left(\tau - \mu\frac{7-5\nu}{15(1-\nu)}\gamma\right) = f_g(\tau - \tau^*_{\text{esh}}), \tag{68}$$

where τ is the applied resolved shear stress and $f_g = V_g/V$. Therefore, the associated backstress τ^*_{esh} reads in this case:

$$\tau^*_{\text{esh}} = \mu\frac{7-5\nu}{15(1-\nu)}\gamma. \tag{69}$$

We can notice that the expression of τ^*_{esh} is the same (except its sign) that the one of τ^0_{13} in Eq. (30). Thus, τ^*_{esh} increases linearly with γ but is independent on grain size R. Let us consider a distribution of circular loops as described before. Then, we only take into account a plastification mechanism driven by the average plastic slip over the grain γ where the spatial configuration of the loops does not evolve (i.e. no multiplication of loops). That means that the spacing h between loops remains constant during the plastification of loops and only the Burgers vector magnitude for each loop may vary. We follow the same method as previously to compute the associated backstress τ^* using Eqs. (18), (52), (64) and (66). We find out that:

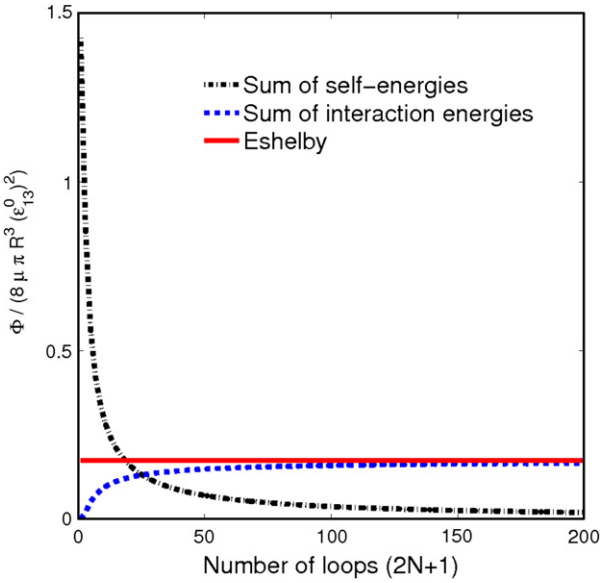

Fig. 13. Evolution of the normalized self-energies and interaction energies for a periodic distribution of single glide dislocation loops as a function of the number of dislocation loops inside the grain ($R = 1\ \mu m$). Comparison with the Eshelby's solution at same average plastic strain over the grain.

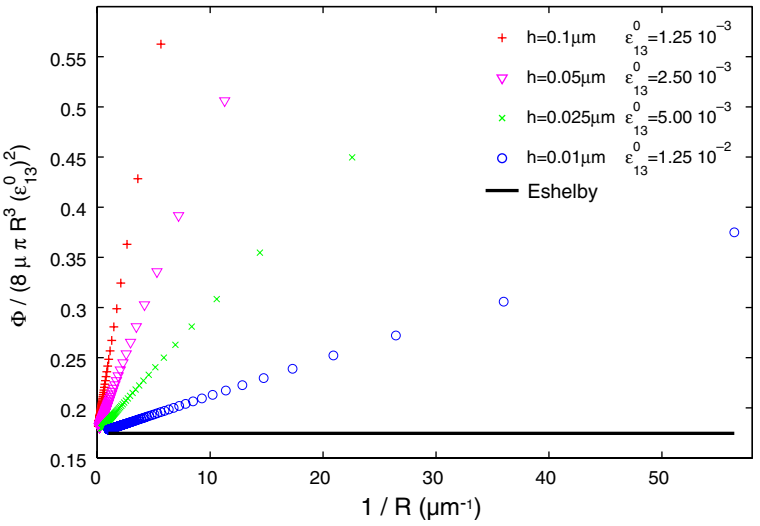

Fig. 14. Evolution of the normalized elastic energy as a function of $1/R$ for constant values of mean plastic strain ϵ^0_{13} and distance h between loops. Comparison with the grain size-independent Eshelby's solution at same average plastic strain over the grain.

$$\tau^* = \tau^*_{\text{esh}} + \alpha'(h)\frac{1}{R}\mu\gamma, \tag{70}$$

where α' is a function depending on h. Fig. 15 displays the evolution of τ^* for three different γ, respectively 0.2%, 0.7% and 2%. Furthermore, Figs. 15(a)–(d) represent four different spatial distributions of loops with the period h being, respectively 0.01, 0.025, 0.05 and 0.1 μm. For comparison, we also report the evolution of τ^*_{esh} with γ. According to Eq. (70) and Fig. 15, the grain size dependence of τ^* scales with $1/R$ with a slope linearly dependent on γ. This is consistent with several experimental data

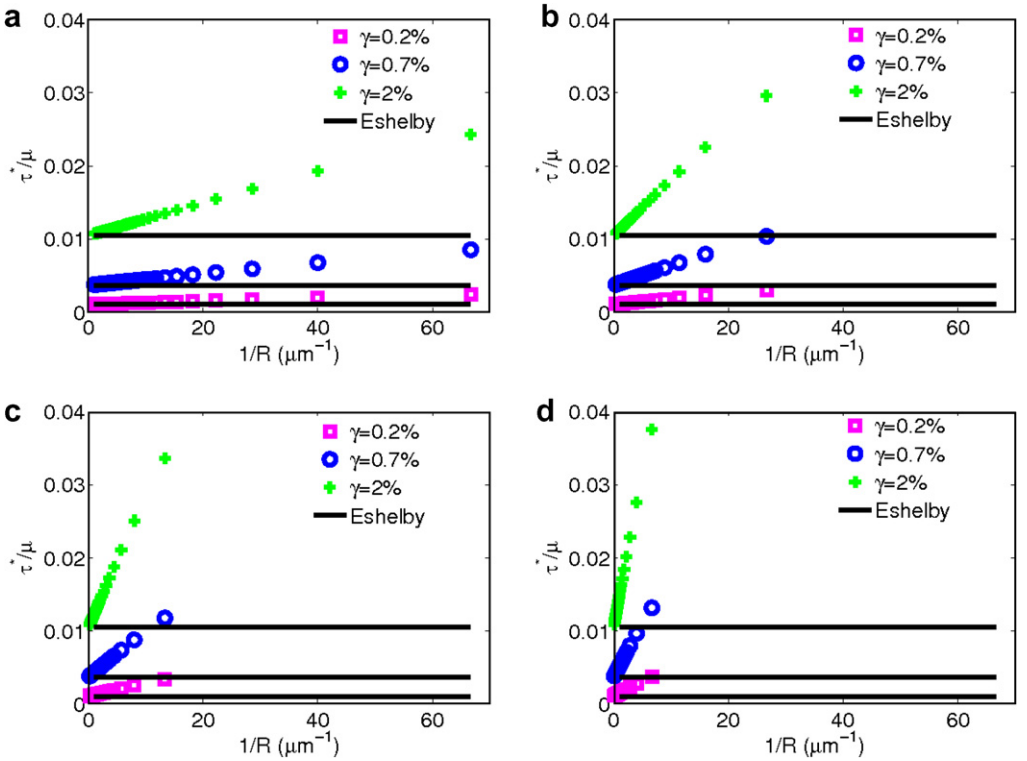

Fig. 15. Evolution of the backstress (normalized with μ) only assuming plastification according to a periodic distribution of single loops as a function of $1/R$ for three different values of average plastic slip over the grain. Various periodic distributions are considered: (a) $h = 0.01$ μm, (b) $h = 0.025$ μm, (c) $h = 0.05$ μm, (d) $h = 0.1$ μm. Comparisons with the grain size-independent Eshelby's solutions at the same average plastic slips over the grain.

on various polycrystalline metals (Hirth, 1972; Dollar and Gorczyca, 1982; Narutani and Takamura, 1991) which reported a linear variation of the flow stress with the inverse of grain size as well as an increasing slope with the plastic strain. Moreover, Figs. 15(a)–(d) highlight the fact that an increase of the period h results in an increase of the slope.

From these calculations, we can interpret the role of this intra-granular microstructure on the flow stress of the polycrystal by considering a Taylor factor (approximately 3 for f.c.c. polycrystals) to account for the distribution of crystallographic orientations in the aggregate and a Schmid flow criterion. Following many experimental data (Hansen and Ralph, 1982; Dollar and Gorczyca, 1982; Hansen, 1985; Narutani and Takamura, 1991; Jiang et al., 1995), we can assume that the macroscopic flow stress Σ_f at any macroscopic plastic strain E^* generally writes as a function of the mean grain size D as follows:

$$\Sigma_f = \Sigma_0(E^*) + K_1 D^{p_1} + K_2(E^*) D^{p_2}. \tag{71}$$

Our model predicts through Eq. (70), that as soon as slip occurs in grains under the form of the considered configurations, then $\Sigma_f = \Sigma_0(E^*) + K_2(E^*)D^{p_2}$ where K_2 contains the Taylor factor, the plastic strain and the exponent p_2 is equal to -1. This means that, the second term $K_1 D^{p_1}$ associated with the grain size dependence of the yield stress $\Sigma_y = \Sigma_0(E^* = 0) + K_1 D^{p_1}$ is not taken into consideration in our model. If $p_1 = -1/2$, the classical Hall–Petch relation (Hall, 1951; Petch, 1953) is retrieved. It is noteworthy that even though pile-up models were identified to explain the Hall–Petch effect (Eshelby et al., 1951; Li and Liu, 1967), other mechanisms can be responsible for this effect (e.g. grain boundary sources). In this paper, the obtained scaling law is related to the elastic energy of the GNDs (Ashby, 1970) located at grain boundaries, as reported in Figs. 8 and 9. This microstructure is different from a pure pile-up model such as the one described by Li and Liu (1967) where the backstress scales with the inverse of the square root of the grain size. It would be interesting to treat in future work distributions of dislocation pile-ups.

The calculated grain size-dependent backstress may also serve to explain the origin of the stronger Bauschinger effect observed when performing reverse loadings on ultrafine-grained materials as revealed experimentally for instance by Vinogradov et al. (1997). The present formalism can also be applied to other types of no penetrable interfaces such as the ones present in passivated freestanding thin films as reported in Nicola et al. (2006).

5.3. Periodic distributions of clusters of loops

We analyze slip configurations consisting in clusters of loops periodically spaced with a given internal distance h_1 and spreading along the direction of **n** as depicted in Fig. 16. These clusters are constituted of dislocations separated each other by another periodic distance h_2 smaller than h_1. The Burgers vectors of the loops are in the (x_1) direction. Such clusters may well reproduce the case of slip bands experimentally observed by Neuhäuser (1983) on slip traces at the surface of deformed metallic single crystals. In the spherical grain of radius R, we assume an odd number $(2P + 1)$ of periodic clusters constrained by a spherical grain boundary. Each of them has a given thickness c (Fig. 16) which is directly deduced from its number of

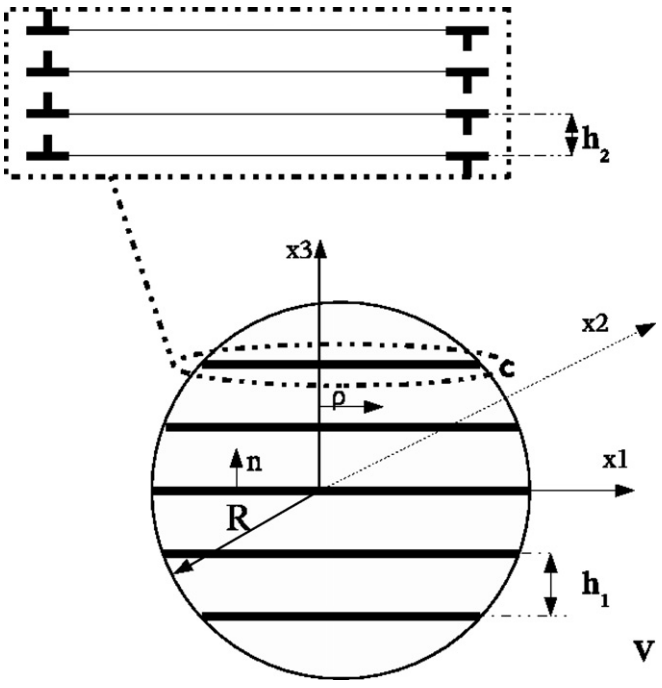

Fig. 16. Spherical grain with radius R and periodic clusters of dislocation loops. Each cluster of constant thickness c contains a given number of loops $2N + 1$ separated by a distance h_2. The clusters are spaced by a distance h_1.

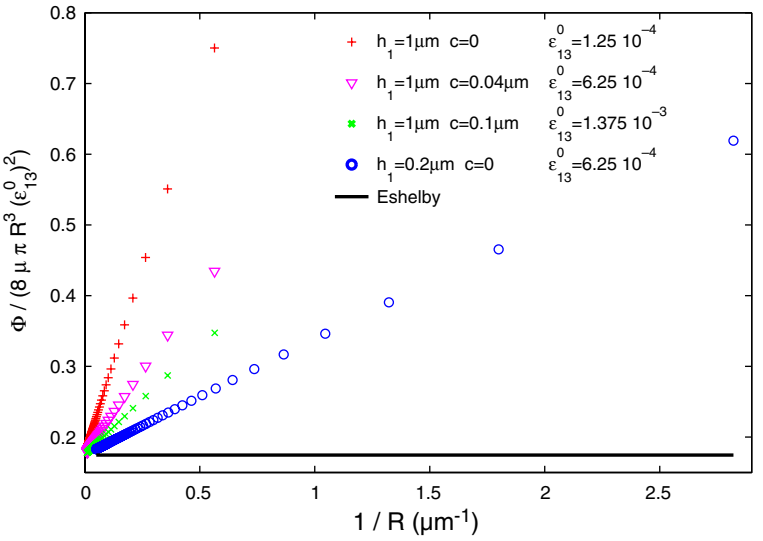

Fig. 17. Evolution of the normalized elastic energy for distributions of clusters of loops as a function of $1/R$ for different band widths c ($c = 0$ corresponds to the case of a periodic distribution of single loops). Comparison with the grain size-independent Eshelby's solution at same average plastic strain over the grain.

loops (assumed odd as well and denoted $2N + 1$) and from h_2. In the present modeling, distance h_2 is kept constant and equal to $40b$ (for this value, dislocation annihilation processes can be disregarded). Thus, the microstructure is characterized by three independent internal lengths: R, h_1 and c. The non-zero plastic distortion component contains the grain radius R and the two spatial periods (h_1, h_2):

$$\beta^*_{31}(\mathbf{x}) = b \sum_{p=-P}^{P} \sum_{n=-N}^{N} H\Big(1 - \frac{\rho}{a^{(n(p))}}\Big)\delta(x_3 - ph_1 - nh_2), \tag{72}$$

where $a^{(n(p))} = \sqrt{R^2 - (ph_1 + nh_2)^2}$ is the radius of the indexed loop n of the indexed cluster p. This loop is located at altitude $x_3 = ph_1 + nh_2$.

The internal elastic energy of these configurations is computed by adding the contributions of the self-energies and the interaction energies between all the $(2N + 1)(2P + 1)$ loops. In the case of clusters of loops, a $1/R$ scaling law for the elastic energy is also retrieved (Fig. 17). This grain size effect is even less pronounced that h_1 is low. In contrast with periodic distributions of single loops ($c = 0$), the grain size effect is also dependent on the band thickness c: decreasing c with a fixed h_1 increases the grain size effect. However, Fig. 17 shows that c has little influence in comparison to h_1. Let us consider for instance a distribution of clusters with constant band thickness $c = 0.04\ \mu m$ and $h_1 = 1\ \mu m$. In this case, at same mean plastic strain, the internal elastic energy exhibits a more pronounced grain size effect than the one derived with a distribution of single loops ($c = 0$) with a lower period $h_1 = 0.2\ \mu m$. What matters here is the spatial scatter of plastic distorsion inside the grain: the grain size effect is even more pronounced as plastic activity is non-uniformly distributed. According to this result, the localization of plastic activity along slip bands should enhance the grain size effect on the overall material's behavior.

6. Conclusions and perspectives

Intra-granular plastic slip heterogeneities have been modeled by periodic distributions of circular glide dislocation loops for a grain embedded in an infinite elastic matrix. Then, field equations and free energy have been solved using the method of Fourier transforms. Presented results show a strong discrepancy of internal stresses with the Eshelby's solution especially in a grain boundary layer. As the number of loops increases, the thickness of this layer decreases and the classic Eshelby's result is retrieved. These new insights determined through a micro-mechanics-based approach are consistent with the numerous experimental observations reporting different behaviors and dislocation structures between near grain boundary regions and grain interior. On the static viewpoint, the present modeling reports strong stress gradients in the grain boundary layer. Because of such gradients, the relaxation of internal stresses during plastification will lead to different microstructures between grain boundary region and grain core. In this paper, we have also taken into consideration the curvature of the interface between the grain and the matrix by examining arrays of circular loops in a spherical grain. Consequently, a natural grain size effect is sketched out from our calculations. In the case of planar arrays, a boundary layer close to interface is also present but no grain size effect can be determined. In the present contribution, a grain size effect has been reported regarding the elastic energy which is normalized to be compared with the Eshelby's result. This one is found to scale with the inverse of the grain size whereas the Eshelby's solution is grain size independent. From our calculations, it is noticeable that

the observed grain size effect arises for a constant periodic distance between loops. This supports the idea of grain size independent spacing between slip bands. At this point, some experimental investigations are needed to accurately quantify the evolution of slip band spacing with grain size. In future, we will consider non-necessary periodic distributions of loops and situations of multiple slip by increasing the number of internal variables (i.e. the degree of freedom of dislocations). Lastly, a more general statistical theory accounting for intra- and inter-granular heterogeneities will be developed.

Acknowledgement

The authors are grateful to the French Agence Nationale de la Recherche (ANR) under contract "LIOM" for financial support.

Appendix A. Derivation of the Helmholtz free energy for a solid with eigenstrains

The Helmholtz free energy per unit volume depends on the imposed macroscopic strain E_{ij} and the plastic strain ϵ^*_{ij} inside the medium. It reads:

$$\phi(E_{ij},\epsilon^*_{ij}(\mathbf{x})) = \frac{1}{V}\int_V \frac{1}{2}\sigma_{ij}(\mathbf{x})\epsilon^{\mathrm{e}}_{ij}(\mathbf{x})\,\mathrm{d}V, \tag{A.1}$$

then, introducing the plastic strain, Eq. (A.1) is transformed into:

$$\phi(E_{ij},\epsilon^*_{ij}(\mathbf{x})) = \frac{1}{V}\int_V \frac{1}{2}\sigma_{ij}(\mathbf{x})(u_{i,j}(\mathbf{x}) - \epsilon^*_{ij}(\mathbf{x}))\,\mathrm{d}V. \tag{A.2}$$

Performing successively an integration by parts, using stress equilibrium and applying the divergence theorem leads to:

$$\phi(E_{ij},\epsilon^*_{ij}(\mathbf{x})) = \frac{1}{2V}\int_{\partial V}\sigma_{ij}(\mathbf{x})u_i(\mathbf{x})n_j\,\mathrm{d}S - \frac{1}{2V}\int_V \sigma_{ij}(\mathbf{x})\epsilon^*_{ij}(\mathbf{x})\,\mathrm{d}V, \tag{A.3}$$

where n_j denotes the outward unit normal to ∂V. On ∂V, a linear displacement field $u^{\mathrm{d}}_i = E_{ij}x_j$ is imposed, then:

$$\phi(E_{ij},\epsilon^*_{ij}(\mathbf{x})) = \frac{1}{2V}\int_{\partial V}\sigma_{ij}(\mathbf{x})E_{ik}x_k n_j\,\mathrm{d}S - \frac{1}{2V}\int_V \sigma_{ij}(\mathbf{x})\epsilon^*_{ij}(\mathbf{x})\,\mathrm{d}V. \tag{A.4}$$

Applying a second time the divergence theorem and simplifying by using the stress equilibrium equation yields:

$$\phi\left(E_{ij},\epsilon^*_{ij}(\mathbf{x})\right) = \frac{1}{2V}E_{ik}\int_V \sigma_{ij}(\mathbf{x})\delta_{kj}\,\mathrm{d}V - \frac{1}{2V}\int_V \sigma_{ij}(\mathbf{x})\epsilon^*_{ij}(\mathbf{x})\,\mathrm{d}V = \frac{1}{2V}E_{ik}\int_V \sigma_{ik}(\mathbf{x})\,\mathrm{d}V - \frac{1}{2V}\int_V \sigma_{ij}(\mathbf{x})\epsilon^*_{ij}(\mathbf{x})\,\mathrm{d}V. \tag{A.5}$$

By denoting Σ_{ij} the macroscopic stress response of the system defined by $\Sigma_{ij} = \frac{1}{V}\int_V \sigma_{ij}(\mathbf{x})\,\mathrm{d}V$, we find out:

$$\phi(E_{ij},\epsilon^*_{ij}(\mathbf{x})) = \frac{1}{2}E_{ij}\Sigma_{ij} - \frac{1}{2V}\int_V \sigma_{ij}(\mathbf{x})\epsilon^*_{ij}(\mathbf{x})\,\mathrm{d}V. \tag{A.6}$$

The overall behavior law is $\Sigma_{ij} = C_{ijkl}(E_{kl} - E^*_{kl})$ assuming homogeneous elasticity $\mathbf{C}$ within the medium and a macroscopic averaged plastic strain $E^*_{ij} = \frac{1}{V}\int_V \epsilon^*_{ij}(\mathbf{x})dV$. Thus, introducing the macroscopic behavior law into Eq. (A.6) yields:

$$\phi(E_{ij},\epsilon^*_{ij}(\mathbf{x})) = \frac{1}{2}E_{ij}C_{ijkl}\left(E_{kl} - E^*_{kl}\right) - \frac{1}{2V}\int_V \sigma_{ij}(\mathbf{x})\epsilon^*_{ij}(\mathbf{x})\,\mathrm{d}V. \tag{A.7}$$

Lastly, let us introduce the internal stress $\tau_{ij}(\mathbf{x})$ (due to plastic sources) from the decomposition of the local stress $\sigma_{ij}(\mathbf{x})$ such that $\sigma_{ij}(\mathbf{x}) = \Sigma_{ij} + \tau_{ij}(\mathbf{x})$. Internal stresses are then self-equilibrated. It comes out from Eq. (A.7):

$$\phi\left(E_{ij},\epsilon^*_{ij}(\mathbf{x})\right) = \frac{1}{2}E_{ij}C_{ijkl}(E_{kl} - E^*_{kl}) - \frac{1}{2V}\Sigma_{ij}\int_V \epsilon^*_{ij}(\mathbf{x})\,\mathrm{d}V - \frac{1}{2V}\int_V \tau_{ij}(\mathbf{x})\epsilon^*_{ij}(\mathbf{x})\,\mathrm{d}V, \tag{A.8}$$

and, using a second time the overall behavior law allows us to write the final expression of the Helmholtz free energy par unit volume ϕ:

$$\phi(E_{ij},\epsilon^*_{ij}(\mathbf{x})) = \frac{1}{2}(E_{ij} - E^*_{ij})C_{ijkl}(E_{kl} - E^*_{kl}) - \frac{1}{2V}\int_V \tau_{ij}(\mathbf{x})\epsilon^*_{ij}(\mathbf{x})\,\mathrm{d}V. \tag{A.9}$$

Appendix B. Mathematical integrations of internal stress fields and elastic energy in the Fourier space for glide dislocation loops

B.1. Displacement and stress fields

First, the displacement and stress components of one single circular dislocation glide loop of radius a centered at the origin can be calculated using cylindrical coordinates:

$$dV = \rho\, d\rho\, d\theta\, dx_3,$$

where (ρ, θ, x_3) are defined as follows:

$$x_1 = \rho\cos\theta$$
$$x_2 = \rho\sin\theta$$
$$x_3 = x_3$$
$$\rho = \sqrt{x_1^2 + x_2^2}.$$

Starting from Eq. (38) for displacement components, we proceed the mathematical integration of the last expressions in the cylindrical coordinates of the Fourier space:

$$dV_\xi = d\xi_1\, d\xi_2\, d\xi_3 = q\, d\phi\, dq\, d\xi_3,$$

where:

$$\xi_1 = q\cos\phi$$
$$\xi_2 = q\sin\phi$$
$$\xi_3 = \xi_3$$
$$q = \sqrt{\xi_1^2 + \xi_2^2}$$
$$\xi^2 = \xi_3^2 + q^2.$$

Then, the displacement components write:

$$\begin{aligned}
u_\rho &= \frac{b\cos\theta\,\mathrm{sgn}(x_3)}{4(1-\nu)}\left(2(1-\nu)J(1,0;0) - \frac{|x_3|}{a}J(1,0;1) + \frac{|x_3|}{\rho}J(1,1;0)\right)\\
u_\theta &= \frac{b\sin\theta\,\mathrm{sgn}(x_3)}{4(1-\nu)}\left(-2(1-\nu)J(1,0;0) + \frac{|x_3|}{\rho}J(1,1;0)\right)\\
u_3 &= \frac{b\cos\theta}{4(1-\nu)}\left((1-2\nu)J(1,1;0) + \frac{|x_3|}{a}J(1,1;1)\right).
\end{aligned} \tag{B.1}$$

In the above expressions, $\mathrm{sgn}(x_3) = +1$ for $x_3 > 0$ and $\mathrm{sgn}(x_3) = -1$ for $x_3 < 0$. $J(m,n;p)$ where m, n and p are integers are the so-called Lipschitz–Hankel integrals (Eason et al., 1955; Salamon and Walter, 1979) defined by:

$$J(m,n;p) = \int_0^{+\infty} J_m(Q)J_n(\overline{\rho}Q)e^{-\frac{Q|x_3|}{a}}Q^p\, dQ,$$

with $\overline{\rho} = \rho/a$, $Q = aq$ and $J_m(Q)$ are Bessel functions of integer order m.

Using now the following recurrence relations resulting from the well-known Bessel recurrence formulae (Abramowitz and Stegun, 1970):

$$\frac{\partial}{\partial\rho}J(m,n;p) = \frac{1}{a}J(m,n-1;p+1) - \frac{n}{\rho}J(m,n;p)$$
$$\frac{\partial}{\partial x_3}J(m,n;p) = -\frac{1}{a}\mathrm{sgn}(x_3)J(m,n;p+1),$$

the internal stress fields for one circular glide dislocation of radius a can be easily derived using the Hooke's law in linear elasticity:

$$\begin{aligned}
\tau_{\rho\rho} &= \frac{\mu b\cos\theta\,\mathrm{sgn}(x_3)}{2(1-\nu)}\left(-\frac{2}{a}J(1,1;1) + \frac{|x_3|}{a^2}J(1,1;2) - \frac{|x_3|}{\rho a}J(1,2;1)\right)\\
\tau_{\rho 3} &= \frac{\mu b\cos\theta}{2(1-\nu)}\left(-\frac{1}{a}J(1,0;1) + \frac{|x_3|}{a^2}J(1,0;2) - \frac{|x_3|}{\rho a}J(1,1;1) + \frac{\nu}{\rho}J(1,1;0)\right)\\
\tau_{\rho\theta} &= \frac{\mu b\sin\theta\,\mathrm{sgn}(x_3)}{2(1-\nu)}\left(-\frac{|x_3|}{\rho a}J(1,2;1) + \frac{1-\nu}{a}J(1,1;1)\right)\\
\tau_{\theta\theta} &= \frac{\mu b\cos\theta\,\mathrm{sgn}(x_3)}{2(1-\nu)}\left(\frac{|x_3|}{\rho a}J(1,2;1) - \frac{2\nu}{a}J(1,1;1)\right)\\
\tau_{\theta 3} &= \frac{\mu b\sin\theta}{2(1-\nu)}\left(\frac{1-\nu}{a}J(1,0;1) + \frac{\nu}{\rho}J(1,1;0) - \frac{|x_3|}{\rho a}J(1,1;1)\right)\\
\tau_{33} &= -\frac{\mu b\cos\theta}{2(1-\nu)}\frac{x_3}{a^2}J(1,1;2).
\end{aligned} \tag{B.2}$$

Then, the internal stress fields can be expressed in the cartesian coordinates as follows:

$$
\begin{aligned}
\tau_{11}(\mathbf{x}) &= \frac{\mu b}{2(1-\nu)}\cos\theta \mathrm{sgn}(x_3)\left\{-\frac{2}{a}J(1,1;1)+\frac{|x_3|}{a^2}\left(\cos^2\theta J(1,1;2)+\frac{a}{\rho}(3-4\cos^2\theta)J(1,2;1)\right)\right\}\\
\tau_{13}(\mathbf{x}) &= \frac{\mu b}{2(1-\nu)}\left\{\frac{\nu-1-\nu*\cos^2\theta}{a}J(1,0;1)+\frac{\nu}{\rho}\cos 2\theta J(1,1;0)+\frac{|x_3|}{a^2}\left(\cos^2\theta J(1,0;2)-\frac{a}{\rho}\cos 2\theta J(1,1;1)\right)\right\}\\
\tau_{12}(\mathbf{x}) &= \frac{\mu b}{2(1-\nu)}\sin\theta \mathrm{sgn}(x_3)\left\{-\frac{1-\nu}{a}J(1,1;1)+\frac{|x_3|}{a^2}\left(\cos^2\theta J(1,1;2)-\frac{a}{\rho}(3-4\sin^2\theta)J(1,2;1)\right)\right\}\\
\tau_{22}(\mathbf{x}) &= \frac{\mu b}{2(1-\nu)}\cos\theta \mathrm{sgn}(x_3)\left\{-\frac{2\nu}{a}J(1,1;1)+\frac{|x_3|}{a^2}\left(\sin^2\theta J(1,1;2)-\frac{a}{\rho}(3-4\cos^2\theta)J(1,2;1)\right)\right\}\\
\tau_{23}(\mathbf{x}) &= \frac{\mu b}{4(1-\nu)}\sin 2\theta\left\{\frac{\nu}{a}J(1,2;1)-\frac{|x_3|}{a^2}J(1,2;2)\right\}\\
\tau_{33}(\mathbf{x}) &= -\frac{\mu b}{2(1-\nu)}\cos\theta\frac{x_3}{a^2}J(1,1;2).
\end{aligned}
\tag{B.3}
$$

The stress fields have been numerically computed using the complete elliptic integrals of first kind $\mathbf{K}(k)$ and second kind $\mathbf{E}(k)$(Gradshteyn and Ryzhik, 1965; Abramowitz and Stegun, 1970):

$$
\begin{aligned}
\mathbf{E}(k) &= \int_0^{\frac{\pi}{2}}\left(1-k^2\sin^2\psi\right)^{1/2}\mathrm{d}\psi\\
\mathbf{K}(k) &= \int_0^{\frac{\pi}{2}}\left(1-k^2\sin^2\psi\right)^{-1/2}\mathrm{d}\psi.
\end{aligned}
$$

Following Eason et al. (1955) and Salamon and Walter (1979), the relations between Lipschitz–Hankel integrals, and, $\mathbf{K}(k)$ and $\mathbf{E}(k)$ are:

$$
\begin{aligned}
J(1,1;0) &= \frac{2}{\pi k\overline{\rho}^{1/2}}\left\{\left(1-\frac{k^2}{2}\right)\mathbf{K}(k)-\mathbf{E}(k)\right\}\\
J(1,1;1) &= \frac{k|x_3|/a}{2\pi\overline{\rho}^{3/2}}\left(\frac{1-k^2/2}{k'^2}\mathbf{E}(k)-\mathbf{K}(k)\right)\\
J(1,0;1) &= \frac{k}{2\pi\overline{\rho}^{1/2}}\left\{\frac{k^2\left(1-\overline{\rho}^2-(x_3/a)^2\right)}{4k'^2\overline{\rho}}\mathbf{E}(k)+\mathbf{K}(k)\right\}\\
J(1,0;2) &= \frac{k^3|x_3|/a}{8\pi k'^2\overline{\rho}^{3/2}}\left\{\left(\frac{k^4\left(1-\left(\overline{\rho}^2+(x_3/a)^2\right)^2\right)}{4k'^2\overline{\rho}^2}+3\right)\mathbf{E}(k)-\frac{k^2\left(1-\overline{\rho}^2-(x_3/a)^2\right)}{4\overline{\rho}}\mathbf{K}(k)\right\}\\
J(1,1;2) &= \frac{k}{2\pi\overline{\rho}^{3/2}}\left\{\frac{k^2}{4k'^2\overline{\rho}}\left(\frac{k^4(x_3/a)^2}{k'^2}-(1+\overline{\rho}^2)\right)\mathbf{E}(k)+\left(1-\frac{k^2(x_3/a)^2(2-k^2)}{8k'^2\overline{\rho}}\right)\mathbf{K}(k)\right\}
\end{aligned}
$$

with:

$$
k^2=\frac{4\rho a}{(a+\rho)^2+x_3^2}\quad\text{and}\quad k'^2=1-k^2.
$$

Finally, in order to find out $J(1,2;1)$ and $J(1,2;2)$ in Eq. (B.3), we apply the recurrence relations (Eason et al., 1955):

$$
\begin{aligned}
J(1,2;1) &= \frac{2}{\overline{\rho}}J(1,1;0)-J(1,0;1)\\
J(1,2;2) &= \frac{2}{\overline{\rho}}J(1,1;1)-J(1,0;2).
\end{aligned}
$$

These stress fields were initially found by Salamon and Dundurs (1971, 1977) using a different technique starting from the Papkovich–Neuber potentials for infinitesimal glide loops. The different formulae derived in this Appendix have been checked using the Mathematica software. Furthermore, we also checked numerically the results on internal stress fields considering circular loops composed of small segments and using the formula of a single dislocation segment given in Hirth and Lothe (1982).

B.2. Internal elastic energy

Regarding the internal elastic energy, we start from the expression of the interaction energy between two loops of radii $a^{(n)}$ and $a^{(m)}$ and separated by a distance d (Eq. (63)) to perform the mathematical integration in the cylindrical coordinates of the Fourier space. Then, the interaction energy writes:

$$\Phi_{\text{inter}}^{(nm)} = \frac{\mu b^2 a^{(n)} a^{(m)}}{2\pi} \int_0^{+\infty} \int_{-\infty}^{+\infty} \int_0^{2\pi} \left(\frac{\sin^2 \phi}{\xi_3^2 + q^2} + \frac{2}{1-\nu} \frac{\xi_3^2 \cos^2 \phi}{(\xi_3^2 + q^2)^2} \right) \cos(\mathrm{d}\xi_3) J_1(a^{(n)} q) J_1(a^{(m)} q) q \, \mathrm{d}\phi \, \mathrm{d}\xi_3 \, \mathrm{d}q. \tag{B.4}$$

By integrating first with respect to ϕ using:

$$\int_0^{2\pi} \cos^2 \phi \, \mathrm{d}\phi = \int_0^{2\pi} \sin^2 \phi \, \mathrm{d}\phi = \pi,$$

and, then, with respect to ξ_3 using:

$$\int_{-\infty}^{+\infty} \frac{\cos(\mathrm{d}\xi_3)}{\xi_3^2 + q^2} \mathrm{d}\xi_3 = \pi \frac{\mathrm{e}^{-\mathrm{d}q}}{q},$$
$$\int_{-\infty}^{+\infty} \frac{\xi_3^2 \cos(\mathrm{d}\xi_3)}{(\xi_3^2 + q^2)^2} \mathrm{d}\xi_3 = \frac{\pi}{2} \left(\frac{\mathrm{e}^{-\mathrm{d}q}}{q} - d\mathrm{e}^{-\mathrm{d}q} \right),$$

we find:

$$\Phi_{\text{inter}}^{(nm)} = \mu b^2 a^{(n)} a^{(m)} \frac{2-\nu}{1-\nu} \frac{\pi}{2} \int_0^{+\infty} J_1(a^{(n)} q) J_1(a^{(m)} q) \mathrm{e}^{-\mathrm{d}q} \, \mathrm{d}q - \frac{\mu b^2 a^{(n)} a^{(m)}}{1-\nu} \frac{\pi}{2} \mathrm{d} \int_0^{+\infty} J_1(a^{(n)} q) J_1(a^{(m)} q) \mathrm{e}^{-\mathrm{d}q} q \, \mathrm{d}q. \tag{B.5}$$

Following Eason et al. (1955), some relevant identities can be used to express the last integrals as complete elliptic integrals of first kind $\mathbf{K}(k)$ and second kind $\mathbf{E}(k)$:

$$\int_0^{+\infty} J_1(a^{(n)} q) J_1(a^{(m)} q) \mathrm{e}^{-\mathrm{d}q} \, \mathrm{d}q = \frac{2}{\pi k \sqrt{a^{(n)} a^{(m)}}} \left(\left(1 - \frac{k^2}{2} \right) \mathbf{K}(k) - \mathbf{E}(k) \right),$$
$$\int_0^{+\infty} J_1(a^{(n)} q) J_1(a^{(m)} q) \mathrm{e}^{-\mathrm{d}q} q \, \mathrm{d}q = \frac{kd}{2\pi (a^{(n)} a^{(m)})^{3/2}} \left(\left(1 - \frac{k^2}{2} \right) (1-k^2)^{-1} \mathbf{E}(k) - \mathbf{K}(k) \right),$$

where:

$$k^2 = \frac{4 a^{(n)} a^{(m)}}{(a^{(n)} + a^{(m)})^2 + d^2}.$$

Thus:

$$\Phi_{\text{inter}}^{(nm)} = \mu b^2 \sqrt{a^{(n)} a^{(m)}} \frac{2-\nu}{1-\nu} \frac{1}{k} \left(\left(1 - \frac{k^2}{2} \right) \mathbf{K}(k) - \mathbf{E}(k) \right) - \frac{\mu b^2}{4} \frac{1}{\sqrt{a^{(n)} a^{(m)}}} \frac{d^2 k}{1-\nu} \left(\left(1 - \frac{k^2}{2} \right) \left(1 - k^2 \right)^{-1} \mathbf{E}(k) - \mathbf{K}(k) \right). \tag{B.6}$$

From the last expression, the self-energy of one dislocation loop of radius a is computed as half the interaction energy between two identical loops separated by a distance $2r_c$. A good approximation of the contribution to the self-energy from the dislocation core can be obtained by setting $r_c = 0.5b$ following DeWit (1960). According to Ghoniem and Sun (1999), based on atomistic calculations, this contribution represents 5–10% of the self-energy. This value (which is also called core cut-off radius) is an *ad-hoc* parameter used to regularize the elastic energy of the loop (Hirth and Lothe, 1982). As shown by LeSar (2004) and Lothe and Hirth (2005), the choice of a relevant core cut-off parameter as a function of the dislocation character should be necessary. Other procedures can be applied to regularize the elastic strain energy such as the Peierls potential (Koslowski et al., 2002). A recent contribution due to Cai et al. (2006) is to consider a non-singular dislocation plastic field to make the thermodynamic force self-consistent with the Peach–Koehler force. These are not the scope of the present study and we limit ourselves to the introduction of a core cut-off parameter which will be adjusted to roughly evaluate the core contribution. Thus, from Eq. (B.6), the self-energy Φ_{self} of one circular glide dislocation loop is approximated by:

$$\Phi_{\text{self}} = \frac{\mu b^2}{2} a \frac{2-\nu}{1-\nu} \frac{1}{k} \left(\left(1 - \frac{k^2}{2} \right) \mathbf{K}(k) - \mathbf{E}(k) \right), \tag{B.7}$$

where:

$$k^2 = \frac{a^2}{a^2 + r_c^2}. \tag{B.8}$$

References

Abramowitz, M., Stegun, I.A., 1970. Handbook of Mathematical Functions, nineth ed. Dover Publications Inc., New York.

Aifantis, E.C., 1987. The physics of plastic deformation. International Journal of Plasticity 3, 211–247.

Aifantis, E.C., 1992. On the role of gradients in the localization of deformation and fracture. International Journal of Engineering Science 30, 1279–1299.

Aifantis, E.C., 1995. Pattern formation in plasticity. International Journal of Engineering Science 33, 2161–2178.

Ashby, M.F., 1970. The deformation of plastically non-homogeneous materials. Philosophical Magazine 21, 399–424.

Berbenni, S., Favier, V., Berveiller, M., 2007a. Impact of the grain size distribution on the behaviour of heterogeneous materials. International Journal of Plasticity 23, 114–142.

Berbenni, S., Favier, V., Berveiller, M., 2007b. Micro–macro modelling of the effects of the grain size distribution on the plastic flow stress of heterogeneous materials. Computational Materials Science 39, 96–105.
Berbenni, S., Favier, V., Lemoine, X., Berveiller, M., 2004. Micromechanical modeling of the elastic–viscoplastic behavior of polycrystalline steels having different microstructures. Materials Science and Engineering A 372, 128–136.
Brinck, A., Engelke, C., Kopmann, W., Neuhäuser, H., 1997. Structure and development of slip lines during plastic deformation of the intermetallic phases fe3al and cuzn. Materials Science and Engineering A, 180–187.
Bullough, R., Bilby, B.A., 1956. Continuous distributions of dislocations and the crystallography of martensitic transformation. Proceedings of the Physical Society B 69, 1276–1286.
Cai, M., Levine, L.E., Langford, S.C., Dickinson, J.T., 2005. Observation of dislocation motion in single crystal and polycrystalline aluminum during uniaxial deformation using photoemission technique. Materials Science and Engineering A, 476–480.
Cai, W., Arsenlis, A., Weinberger, C.R., Bulatov, V.V., 2006. A non-singular theory of dislocations. Journal of the Mechanics and Physics of Solids 54, 561–587.
DeWit, R., 1960. The continuum theory of stationary dislocations. Solid State Physics 10, 269–292.
Dollar, M., Gorczyca, S., 1982. The effect of grain size on polycrystal hardening. Scripta Materialia 16, 901–906.
Eason, G., Noble, B., Sneddon, I.N., 1955. On certain integrals of Lipschitz–Hankel type involving products of bessel functions. Philosophical Transactions of the Royal Society of London A. Mathematical and Physical Sciences 247 (935), 529–551.
Eshelby, J.D., Frank, F.C., Nabarro, F.R.N., 1951. The equilibrium of linear arrays of dislocations. Philosophical Magazine 42, 351–364.
Eshelby, J.D., 1957. The determination of the elastic field of an ellipsoidal inclusion and related problems. Proceedings of the Royal Society London A 241, 376–396.
Eshelby, J.D., 1959. The elastic field outside an ellipsoidal inclusion. Proceedings of the Royal Society London A 252, 561–569.
Essmann, U., Mughrabi, H., 1979. Annihilation of dislocations during tensile and cyclic deformation and limits of dislocation densities. Philosophical Magazine A 40 (6), 731–756.
Forest, S., Barbe, F., Cailletaud, G., 2000. Cosserat modelling of size effects in the mechanical behaviour of polycrystals and multi-phase materials. International Journal of Solids and Structures 37, 7105–7126.
Fréchard, S., Martin, F., Clément, C., Cousty, J., 2006. Afm and ebsd combined studies of plastic deformation in a duplex stainless steel. Materials Science and Engineering A 418, 312–319.
Ghoniem, N.M., Sun, L.Z., 1999. Fast-sum method for the elastic field of three-dimensional dislocation ensembles. Physical Review B 60 (1), 128–140.
Gradshteyn, I.S., Ryzhik, I.M., 1965. Table of Integrals, Series and Products. Academic Press Inc., New York.
Hall, E.O., 1951. The deformation and ageing of mild steel: Iii. discussion of results. Proceedings of the Physical Society B 64, 747–753.
Hansen, N., Ralph, B., 1982. The strain and grain size dependence of the flow stress of copper. Acta Metallurgica 30, 411–417.
Hansen, N., 1985. Polycrystalline strengthening. Metallurgical Transactions A 16, 2167–2190.
Hirth, J.P., Lothe, J., 1982. Theory of Dislocations. Wiley, New York.
Hirth, J.P., 1972. The influence of grain boundaries on mechanical properties. Metallurgical Transactions 3, 3047–3067.
Jiang, Z., Lian, J., Baudelet, B., 1995. A dislocation density approximation for the flow stress-grain size relation of polycrystals. Acta Metallurgica and Materialia 43 (9), 3349–3360.
Ju, J.W., Sun, L.Z., 1999. A novel formulation for the exterior point Eshelby's tensor of an ellipsoidal inclusion. ASME Journal of Applied Mechanics 66, 570–574.
Khraishi, T.A., Hirth, J.P., Zbib, H.M., Khaleel, M.A., 2000. The displacement, and strain–stress fields of a general circular Volterra dislocation loop. International Journal of Engineering Science 38, 251–266.
Khraishi, T.A., Zbib, H.M., 2002. Dislocation dynamics simulations of the interaction between a short rigid fiber and a glide circular dislocation pile-up. Computational Materials Science 24, 310–322.
Kosevich, A.M., 1979. Crystal dislocations and the theory of elasticity. In: Nabarro, F.R.N. (Ed.), Dislocations in Solids, vol. 1. North-Holland, Amsterdam, pp. 33–141 (Chapter 1).
Koslowski, M., Cuitiño, A.M., Ortiz, M., 2002. A phase-field theory of dislocation dynamics, strain hardening and hysteresis in ductile single crystals. Journal of the Mechanics and Physics of Solids 50, 2597–2635.
Kröner, E., 1958. Kontinuumstheorie der Versetzungen und Eigenspannungen. Springer-Verlag, Berlin.
Kröner, E., 1960. Allgemeine kontinuumstheorie der versetzungen eigenspannungen. Archive for Rational Mechanics and Analysis 4 (1), 273–334.
Kröner, E., 1966. Dislocation field theory. In: Theory of Crystal Defects. Academia, Czech. Academy of Sciences, Prague, pp. 231–256.
Kröner, E., 1981. Continuum theory of defects. In: Balian, R., et al. (Eds.), Physics of Defects. Les Houches, Session 35. North Holland, New York, pp. 215–315.
Kroupa, F., 1962. Continuous distribution of dislocations loops. Czechoslovak Journal of Physics B12, 191–201.
Kubin, L.P., Canova, G., Condat, M., Devincre, B., Pontikis, V., Bréchet, Y., 1992. Dislocation microstructures and plastic flow: a 3d simulation. Solid State Phenomena, 455–472.
LeSar, R., 2004. Ambiguities in the calculation of dislocation self-energies. Physica Status Solidi (b) 241 (13), 2875–2880.
Li, J.C.M., Liu, G.C.T., 1967. Circular dislocation pile-ups i. strength of ultra-fine polycrystalline aggregates. Philosophical Magazine 15, 1059–1063.
Lothe, J., Hirth, J.P., 2005. Dislocation core parameters. Physica Status Solidi (b) 242 (4), 836–841.
Margolin, H., Stanescu, M.S., 1975. Polycrystalline strengthening. Acta Metallurgica 23, 1411–1418.
Miguel, M.C., Vespignani, A., Zapperi, S., Weiss, J., Grasso, J.R., 2001. Intermittent dislocation flow in viscoplastic deformation. Nature 410, 667–671.
Mura, T., 1964. Periodic distributions of dislocations. Proceedings of the Royal Society London A 280, 528–544.
Mura, T., 1987. Micromechanics of Defects in Solids. Kluwer Academic Publishers, Dordrecht, The Netherlands.
Narutani, T., Takamura, J., 1991. Grain size strengthening in terms of dislocation density measured by resistivity. Acta Metallurgica 39, 2037–2049.
Nemat-Nasser, S., Hori, M., 1993. Micromechanics: overall properties of heterogeneous materials. North-Holland.
Neuhäuser, H., 1983. Slip-line formation and collective dislocation motion. In: Nabarro, F.R.N. (Ed.), Dislocations in Solids, vol. 4. North-Holland, Amsterdam, pp. 319–440.
Nicola, L., Xiang, Y., Vlassak, J., VanderGiessen, E., Needleman, A., 2006. Plastic deformation of freestanding thin films: experiments and modeling. Journal of the Mechanics and Physics of Solids 54, 2089–2110.
Nye, J.F., 1953. Some geometrical relations in dislocated crystals. Acta Metallurgica 1, 153–162.
Peach, M., Koehler, J.S., 1950. The forces exerted on dislocations and the stress fields produced by them. Physical Review 80 (3), 436–439.
Petch, N.J., 1953. The cleavage strength of polycrystals. Journal of the Iron and Steel Institute 174, 25–28.
Rey, C., Saada, G., 1976. The elastic field of periodic dislocation networks. Philosophical Magazine 33 (5), 825–841.
Richeton, T., Dobron, P., Chmelik, F., Weiss, J., Louchet, F., 2006. On the critical behaviour of plasticity in metallic single crystals. Materials Science and Engineering A 424, 190–195.
Richeton, T., Weiss, J., Louchet, F., 2005. Breakdown of avalanche critical behaviour in polycrystalline plasticity. Nature Materials 4, 465–469.
Saada, G., Bouchaud, E., 1993. Dislocation walls. Acta Metallurgica and Materialia 41 (7), 2173–2178.
Saada, G., 1979. Elastic field of dislocation networks and grain boundaries. Acta Metallurgica 27, 921–931.
Saada, G., 2006. Planar dislocation arrays and crystal plasticity. In: Buschow, K.H.J. et al. (Eds.), Encyclopedia of Materials: Science and Technology. Elsevier, pp. 1–18.
Sabar, H., Berveiller, M., Favier, V., Berbenni, S., 2002. A new class of micro–macro models for elastic–viscoplastic heterogeneous materials. International Journal of Solids and Structures 39, 3257–3276.
Salamon, N.J., Dundurs, J., 1971. Elastic fields of a dislocation loop in a two-phase material. Journal of Elasticity 1, 153–164.
Salamon, N.J., Dundurs, J., 1977. A circular glide dislocation loop in a two-phase material. Journal of Physics C: Solid State Physics 10, 497–507.

Salamon, N.J., Walter, G.G., 1979. Limits of Lipschitz–Hankel integrals. IMA Journal of Applied Mathematics 24 (3), 237–254.
Schwarz, K.W., 1999. Simulation of dislocations on the mesoscopic scale i. methods and examples. Journal of Applied Physics 85 (1), 108–119.
Shu, J.Y., Fleck, N.A., 1999. Strain gradient crystal plasticity: size-dependent deformation of bi-crystals. Journal of the Mechanics and Physics of Solids 47, 297–324.
Verdier, M., Fivel, M., Groma, I., 1998. Mesoscopic scale simulation of dislocation dynamics in f.c.c. metals: principles and applications. Modelling and Simulation in Materials Science Engineering 6, 755–770.
Villechaise, P., Sabatier, L., Girard, J., 2002. On slip band features and crack initiation in fatigued 316l austenitic stainless steel: Part 1: analysis by electron back-scattered diffraction and atomic force microscopy. Materials Science and Engineering A 323, 377–385.
Vinogradov, A., Kaneko, Y., Kitagawa, K., Hashimoto, S., Stolyarov, V., Valiev, R., 1997. Cyclic response of ultrafine-grained copper at constant plastic strain amplitude. Scripta Materialia 36 (11), 1345–1351.
Volterra, V., 1907. Sur l'équilibre des corps élastiques multiplement connexes. Annales des Sciences de l'Ecole Normale Supérieure de Paris 24, 401–517.
Zaiser, M., Aifantis, E.C., 2006. Randomness and slip avalanches in gradient plasticity. International Journal of Plasticity 22, 1432–1455.
Zaiser, M., Grasset, F.M., Koutsos, V., Aifantis, E.C., 2004. Self-affine surface morphology of plastically deformed metals. Physical Review Letters 93, 195507.
Zaiser, M., Seeger, A., 2002. Long-range internal stresses, dislocation patterning and work-hardening in crystal plasticity. In: Nabarro, F.R.N., Duesbery, M.S. (Eds.), Dislocations in Solids, vol. 11. North-Holland, Amsterdam, pp. 1–100.